REVIEWS

Journal of Semiconductors
(2021) 42, 101607
doi: 10.1088/1674-4926/42/10/101607

Recent advances and prospects of asymmetric non-fullerene small molecule acceptors for polymer solar cells

Liu Ye[1], Weiyu Ye[1], and Shiming Zhang[1, 2, †]

[1]Key Laboratory of Flexible Electronics (KLOFE) & Institute of Advanced Materials (IAM), Jiangsu National Synergetic Innovation Center for Advanced Materials (SICAM), Nanjing Tech University, Nanjing 211816, China

[2]Jiangsu Seenbom Flexible Electronics Institute Co. Ltd., Nanjing 210043, China

Abstract: Recently, polymer solar cells developed very fast due to the application of non-fullerence acceptors. Substituting asymmetric small molecules for symmetric small molecule acceptors in the photoactive layer is a strategy to improve the performance of polymer solar cells. The asymmetric design of the molecule is very beneficial for exciton dissociation and charge transport and will also fine-tune the molecular energy level to adjust the open-circuit voltage (V_{oc}) further. The influence on the absorption range and absorption intensity will cause the short-circuit current density (J_{sc}) to change, resulting in higher device performance. The effect on molecular aggregation and molecular stacking of asymmetric structures can directly change the microscopic morphology, phase separation size, and the active layer's crystallinity. Very recently, thanks to the ingenious design of active layer materials and the optimization of devices, asymmetric non-fullerene polymer solar cells (A-NF-PSCs) have achieved remarkable development. In this review, we have summarized the latest developments in asymmetric small molecule acceptors (A-NF-SMAs) with the acceptor–donor–acceptor (A–D–A) and/or acceptor–donor–acceptor–donor–acceptor (A–D–A–D–A) structures, and the advantages of asymmetric small molecules are explored from the aspects of charge transport, molecular energy level and active layer accumulation morphology.

Key words: polymer solar cells; non-fullerene acceptors; small asymmetric molecules

Citation: L Ye, W Y Ye, and S M Zhang, Recent advances and prospects of asymmetric non-fullerene small molecule acceptors for polymer solar cells[J]. *J. Semicond.*, 2021, 42(10), 101607. http://doi.org/10.1088/1674-4926/42/10/101607

1. Introduction

Owing to the flexibility, portability, transparency, and low manufacturing cost, polymer solar cells (PSCs) have great potential for commercial production and application[1–6]. The active layer of PSCs mainly adopts a bulk heterojunction structure with a blend of polymer donors and non-fullerene small molecule acceptors (NF-SMAs)[7]. Compared with fullerene acceptors, the advantages of non-fullerene small molecule acceptors include[8–12]: (1) Structural modularity facilitates molecular tailoring and property regulation; (2) Strong intramolecular charge transfer (ICT) enhances the absorption of visible light; (3) The planar molecular skeleton is conducive to charge transport; (4) Side chains prevent molecules excessive aggregation; (5) Non-spherical configuration is conducive to morphological stability. In addition, PSCs have the advantages of good film-forming properties, so their power conversion efficiencies (PCEs) are relatively high, so PSCs are currently the mainstream research direction of organic solar cells (OSCs)[13, 14]. Until now, the highest energy conversion efficiency of PSCs has reached 18.22%[13], far exceeding the 10% PCE commercial bottleneck.

From 2011–2014, plenty of NF-SMAs have been designed with various electron-withdrawing groups such as indanedione[1], dicyannovinyl[2–4], benzothiadiazole[5, 6], diketopyrolopyrrole[7, 15], and arylene diimide[16, 17]. With the unremitting efforts of Zhan Xiaowei's group, 2,2'-[[6,6,12,12-tetrakis (4-hexylphenyl)-s-indacenodithieno[3,2-b]thiophene]methylidyne(3-oxo-1H-indene-2,1(3H)-diylidene)]]bis(propanedinitrile) (ITIC) and 2,2'-2,2'-[(4,4,9,9-tetrahexyl-4,9-dihydro-s-indaceno[1,2-b:5,6-b']dithiophene-2,7-diyl)bis[methylidyne(3-oxo-1H-indene-2,1(3H)-diylidene)]]bis[propanedinitrile] (IDIC) (Fig. 1(b)) were reported in 2015 and 2017 respectively, which opened a new chapter in the research of PSCs[14, 18]. A series of works have been reported, and the related research results are greatly conducive to the in-depth understanding of PSCs, thus promoting the rapid development of industrial research. According to structural characteristics, NF-SMAs can divide into symmetrical and asymmetrical structures. Thanks to the researchers for their continuous exploration and research, many research results and breakthroughs have been made in symmetric non-fullerene small molecule acceptors (S-NF-SMAs) and asymmetric non-fullerene small molecule acceptors (A-NF-SMAs) in recent years.

The asymmetric design of the molecule helps increase the dipole moment and dielectric constant and reduces the exciton binding energy, which is very beneficial to exciton dissociation and charge transport[19–21]. Simultaneously, compared with the S-NF-SMAs, the asymmetric design of A-NF-SMAs will finely regulate the molecular energy level, thereby further adjusting the open-circuit voltage (V_{oc}). Changes in the absorption range and absorption intensity will cause the short-circuit current density (J_{sc}) to change accordingly. The influence of molecular aggregation and molecular accumulation can directly change the microsco-

Correspondence to: S M Zhang, iamsmzhang@njtech.edu.cn
Received 29 JUNE 2021; Revised 6 SEPTEMBER 2021.

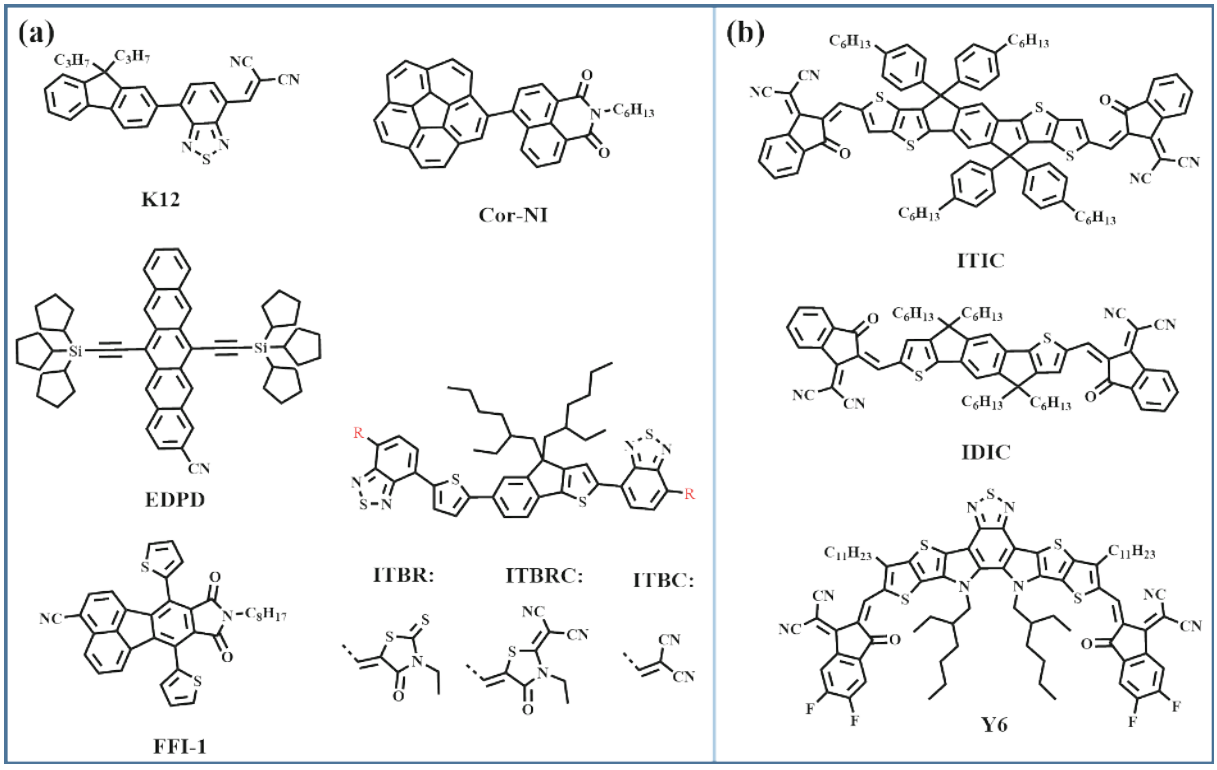

Fig. 1. Chemical structures of (a) early reports of A-NF-SMAs, (b) early reports of small molecule acceptors.

pic morphology, phase separation, and trap degree of the active layer[22, 23].

Generally speaking, V_{oc} and J_{sc} are two iconic device performance parameters, and the increase of the value of $V_{oc} \times J_{sc}$ generally shows the improvement of device performance. Further optimize the value of $V_{oc} \times J_{sc}$ through asymmetric molecular design to obtain higher device performance, which provides the latest research ideas and unique insights for PSCs research[22]. So far, the maximum power conversion efficiency (PCE_{max}) of PSCs based on asymmetric non-fullerene acceptors has gradually increased from 0.73% in 2011 to more than 17% in 2020. The development of A-NF-SMAs can be traced back to 2011. Paul Meredith's research group published asymmetric donor–acceptor typed small molecule acceptor K12 and John E. Anthony's research group published a series of asymmetric electron-deficient pentacene acceptors (Fig. 1(a)). K12 and these deficient pentacene acceptors are blended with P3HT as the polymer donor to fabricate binary PSCs, and the highest PCE of PSCs obtained reaches 0.73% and 1.27%, respectively[25, 26]. In 2012, Pei's research team designed and synthesized an A-NF-SMA (FFI-1) (Fig. 1(a))[27], with polymer donor P3HT and fullerene acceptor PCBM to produce a ternary system PSC. This device produced a breakthrough PCE of 4.1%. In 2014, Cao and coworkers developed an asymmetric non-fullerene SMA, Cor-NI, by introducing the electron-withdrawing n-hexylnaphthalimide moiety part into the C5-symmetric corannulene core[28]. PSCs with P3HT:Cor-NI as the active layer material achieved a PCE of 1.03%. However, during the three years from 2014 to 2017, there was no research related to A-NF-SMAs. Until 2017, Tang *et al.*[29] designed and synthesized three new A-NF-SMAs (ITBC, ITBR, ITBRC) by incorporating indenothiophene as the central core. Inverted structure PSCs using ITBR (Fig. 1(a)) as the acceptor and PTB7-Th as the donor material (Fig. 4) afford a PCE_{max} of 7.49%.

There have been related review articles summarizing the latest development of A-NF-SMAs, but its research content focused on the PSCs with a five-membered indaceno[1,2-b:5,6-b']dithiophene (IDT) series of A-NF-SMAs[28]. The newly reported "Y series" NF-SMAs, especially Y6 (Fig. 1(b)), have brought PSCs into a new golden age [30, 31]. Fully applying the asymmetric structural design concept, researchers have studied many A-NF-SMAs based on the "Y series" structure to achieve a further breakthrough in PCE_{max}. The highest PCE of binary blended PSCs based on the acceptor–donor–acceptor–donor–acceptor (A–D–A–D–A) typed A-NF-SMAs has reached 17.06%, and the highest PCE of ternary blended PSCs has reached 17.43%[32]. Therefore, there is no doubt that the high-efficiency A-NF-SMAs have had a profound significance in the development of PSCs in the past ten years[30].

This review summarizes asymmetric non-fullerene polymer solar cells (A-NF-PSCs)-related content from three aspects: the structural advantages of the asymmetric system, the development history, and the research results in recent years. Meanwhile, we have also made a particular outlook on future research prospects, hoping to provide some guiding insights on the development of PSCs in the future.

2. Photophysical properties of OSCs

The structure and mechanism of photovoltaic devices have been discussed and studied in many excellent studies[10–12]. Here, we will briefly mention the photophysical mechanism of OSCs and discuss the necessary photophysical performance parameters. The structure of the bulk heterojunction OSCs is composed of a metal cathode, an electron transport layer, an active layer, a hole transport layer and a glass substrate as shown in Figs. 2(b) and 2(c). The photovoltaic ef-

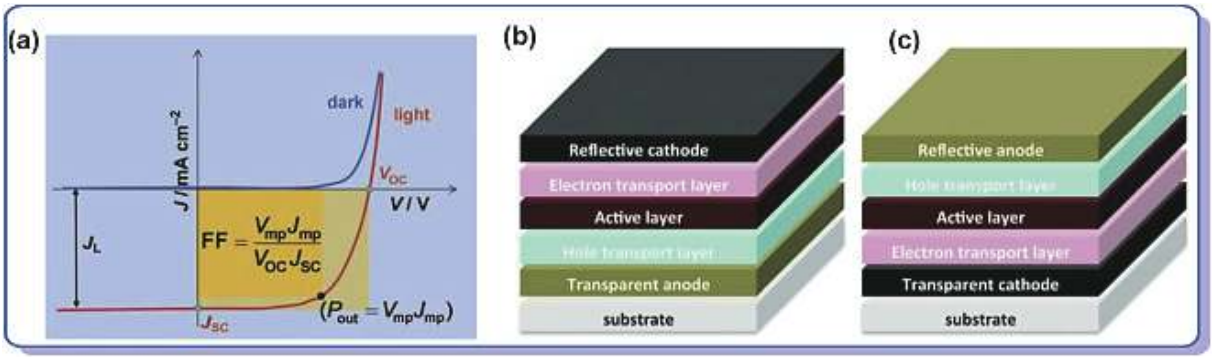

Fig. 2. (a) A typical current–voltage J–V characteristics of solar cells. (b) Standard architecture of bulk-heterojunction (BHJ) and (c) inverted structure. Reproduced with the permission of Ref. [34].

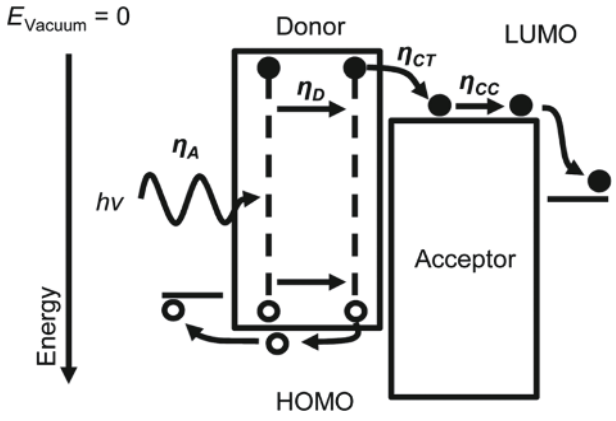

Fig. 3. Simplified schematic of photoconversion in OSCs with the processes of photon absorption, exciton diffusion, exciton dissociation by charge transfer, and charge carrier collection denoted. Reproduced with permission from Ref. [33].

fect is the theoretical basis for the photoelectric conversion process of OSCs. This process mainly occurs in the active layer, including the following processes (Fig. 3)[33]: (1) exciton generation, transport, and dissociation; (2) charge carrier transport; (3) charge carrier collected by electrodes.

The photophysical characteristics of OSCs are generally represented by current density–voltage curves (J–V)[34]. As shown in Fig. 2(a), the main parameters are as follows:

(1) V_{oc}

Under light conditions, V_{oc} is the voltage at which the positive and negative poles of the OSCs are in an open circuit state, that is, the maximum output voltage of the OSCs[27, 28]. In the OSCs composed of donor/acceptor, V_{oc} is directly related to the extreme difference between the donor's highest occupied molecular orbital (HOMO) energy level and acceptor's lowest unoccupied molecular orbital (LUMO) energy. Therefore, the value of V_{oc} can be increased either by reducing the HOMO level of the donor or increasing the LUMO level of the acceptor[34].

(2) J_{sc}

J_{sc} is the current per unit area when the positive and negative electrodes of the OSCs are in a short-circuit state, that is, the maximum output current density of the OSCs in the light environment. As the band-gap of the material decreases, the value of J_{sc} increases and can be affected by the electron and hole transport efficiency of the active material[22, 23].

(3) Fill factor (FF)

FF is a dimensionless physical quantity, which is the ratio of the maximum output power (P_{max}) of the OSCs device to the product of V_{oc} and J_{sc}, which can be expressed by Eq. (1).

$$\mathrm{FF} = \frac{V_{max}J_{max}}{V_{oc}J_{sc}} = \frac{P_{max}}{V_{oc}J_{sc}}. \quad (1)$$

FF is mainly related to the transfer and collection process of charge carriers. The balance of hole/electron mobility in the active layer, the degree of recombination during carrier transport, and the collection efficiency of carriers reaching the buffer layer will all affect the FF value of OSCs. The FF suggests how swiftly the charges can be removed from the cells and the ideal value is 1.0. Several factors can affect the FF of OSCs and they often interact in intricate ways[35].

(4) Power conversion efficiency (PCE)

PCE is the percentage of incident light energy converted into effective electric energy, which can be expressed by the ratio of P_{max} of OSCs to incident power (P_{in}). In this case, the current density and applied bias voltage are expressed by J_{max} and V_{max} respectively, the calculation formula of PCE is as follow[36]:

$$\mathrm{PCE} = \frac{P_{max}}{P_{in}} = \frac{V_{max}J_{max}}{P_{in}} = \frac{V_{oc}J_{sc}\mathrm{FF}}{P_{in}}. \quad (2)$$

It can be seen that the PCE is jointly determined by V_{oc}, J_{sc}, and FF, and represents the ability of OSCs to convert solar energy into electrical energy.

(5) External quantum efficiency (EQE)

The ratio of the number of electrons that can be collected under a certain wavelength of radiation to the number of incident photons at that wavelength can be expressed by the following Eq. (3):

$$\mathrm{EQE} = \frac{1240J_{sc}}{\lambda P_{in}}. \quad (3)$$

Among them, λ is the wavelength of the incident light, and P_{in} is the power of the incident light. EQE is the product of light absorption efficiency, exciton diffusion and dissociation efficiency, charge transfer efficiency, and charge collection efficiency in the photoelectric conversion process. The EQE and J_{sc} can be mutually verified, and high EQE is the prerequisite for realizing high-efficiency OSCs[24].

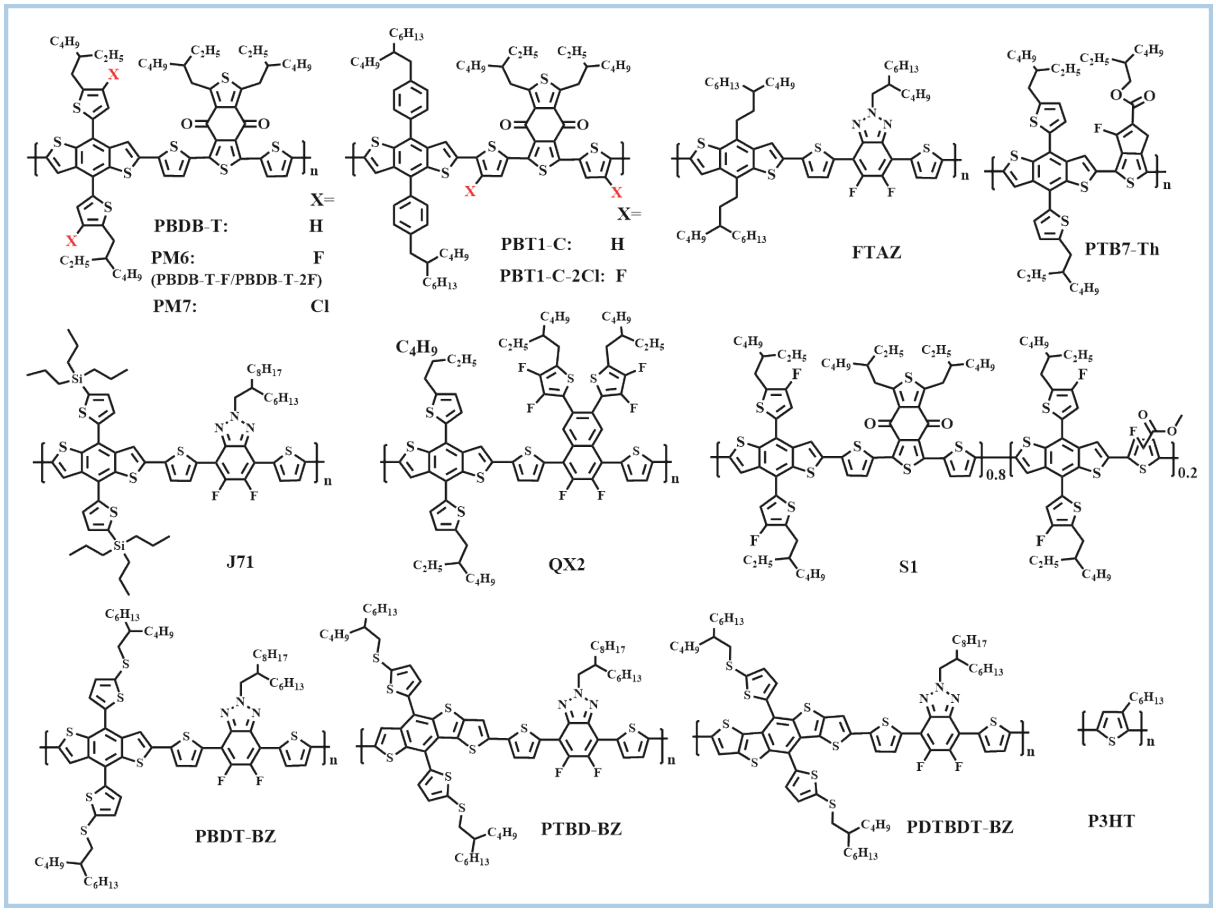

Fig. 4. Chemical structures of polymer donors.

3. Asymmetric non-fullerene acceptors based on A–D–A structures

Previous studies on A-NF-PSCs have been reviewed and published[28]. This review will only introduce some relevant active layer materials with high-efficiency device performance. Fig. 4 shows the related polymer donors.

3.1. A-NF-SMAs with asymmetric cores

The structure of A-D-A is usually composed of one electron-donating unit and two electron-withdrawing units. This push–pull electron behavior in the molecule contributes to ICT so that the molecule has a strong transition dipole and wide spectral absorption range[8]. Generally speaking, molecular asymmetry features mainly include core unit asymmetry, terminal group asymmetry, and side-chain asymmetry. The asymmetry of all parts will cause changes in the intra-molecular dipole moment and intermolecular binding energy, thereby affecting the charge transport and exciton dissociation[21, 28].

In the related research on the asymmetry of the core unit, the dipole moment and arrangement of the molecule can be adjusted by changing the number of asymmetric thiophene units and introducing heavy atoms. In the core unit of electron donation, the IDT core and the heptacyclic indacenodithieno[3,2-b]thiophene (IDTT) core play an important foundational role in the design of high-performance non-fullerene receptors, a new type of asymmetric ladder-type thiophene-phenylenethieno[3,2-b]thiophene-fused (TPTT) core combines the structural features of IDT and IDTT. At the same time, the π conjugate length of TPTT and the electron-donating capacity are all between IDT and IDTT. TPTT-IC (its structure is the same as T-TT), TPTT-2F, T-TT-4F, T-TT-4Cl, IDT6CN and IDT6CN-M are all molecules designed based on the TPTT core (Fig. 5). They have terminal groups which are different from each other. Their maximum absorption wavelengths range from 693 nm to 808 nm, and their LUMO energy levels range from –3.37 to –4.04 eV[37–40]. Finally, the device based on PBDB-T:IDT6CN-M blended film achieved the highest PCE of 11.23%, with a V_{oc} of 0.92 V, a J_{sc} of 15.97 mA/cm^2, and a FF of 76.1%, by using 0.5% diiodooctane (DIO) as a solvent additive and thermal annealing at 100 ℃. Li *et al.* designed the asymmetric molecule TTPT-T-2F by cutting IDTT fragments and synthesized symmetric molecule IT-2F and T-TPT-T-2F. TTPT-T-2F, IT-2F and T-TPT-T-2F were respectively blended with the donor PBT1-C to fabricate PSCs. Thanks to the TTPT-T-2F-based PSCs with the highest J_{sc} value (18.50%), a promising PCE_{max} of 12.71% is achieved for TTPT-T-2F-based PSCs, which outperforms those of devices based on IT-2F (PCE = 10.54%) and T-TPT-T-2F (PCE = 10.71%)[41]. Gao *et al.* realized the optimization of the molecular morphology by introducing the thioenyl side chain, which promoted BHJ active layer to have good characteristics, such as higher and more balanced carrier mobility, tiny bimolecular reorganization, and orderly structure. Finally, the PBDB-T:IDT6CN-Th system achieved a very high FF of 76.72% and a PCE of 10.41%[42, 43]. By further adjusting the terminal groups, IDT6CN-TM has a more significant dipole moment. Compared with IDT6CN-Th and IDT6CN-4F, the strong dipole mo-

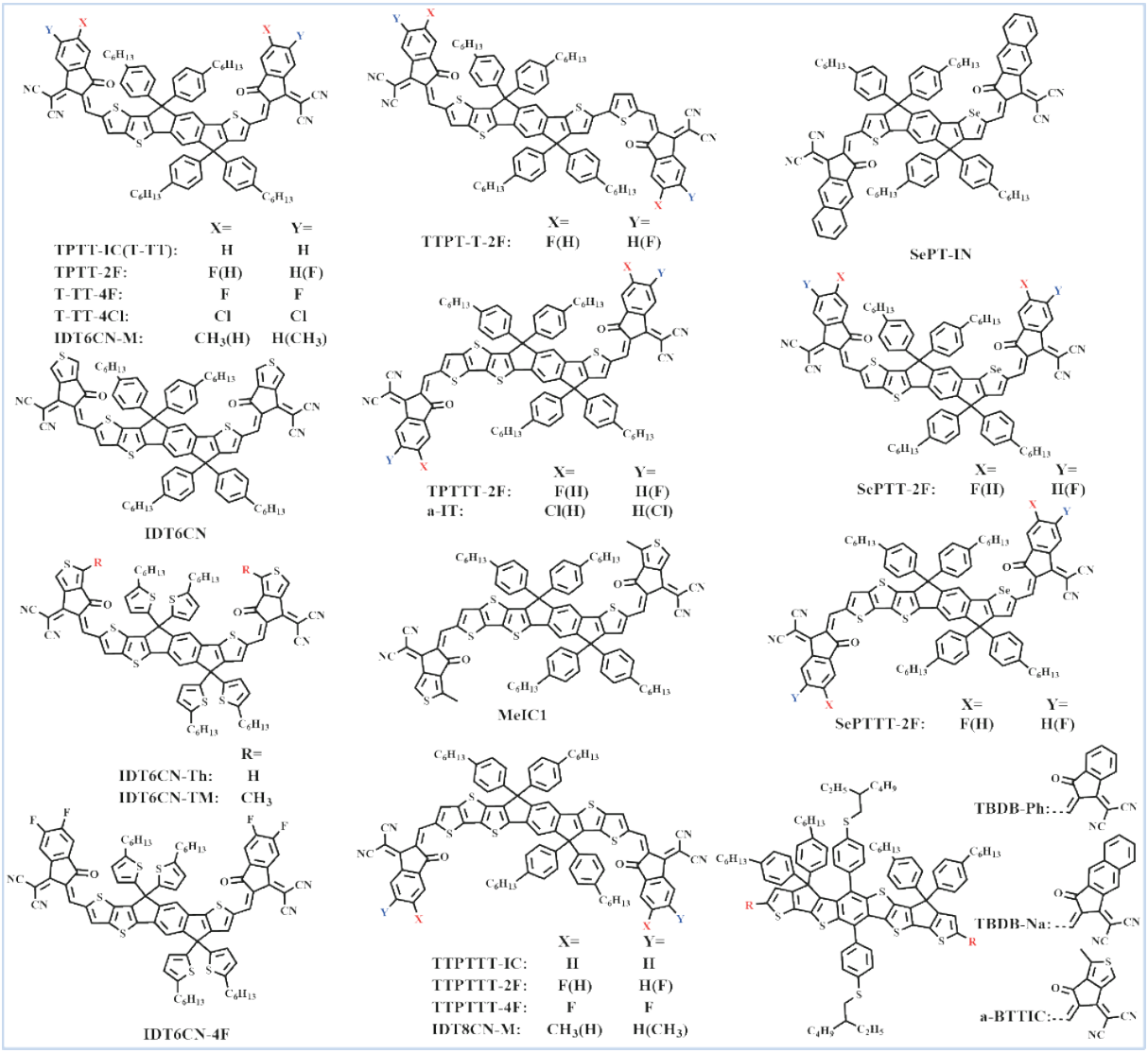

Fig. 5. Chemical structures of A–D–A asymmetric non-fullerene acceptors without nitrogen.

ment contributes more substantial π–π stacking and higher electron mobility of IDT6CN-TM. The devices based on PM6:IDT6CN-TM obtained PCE of 12.4% (V_{oc} = 0.95 V, J_{sc} = 17.40 mA/cm^2, FF = 74.7%), which is currently the highest PCE among non-fullerene PSCs with thienyl side chains.

In the combination of monothiophene and trithiophene, extending the IDT nuclear conjugation length can expand the spectral absorption, shift the LUMO energy level up, and improve electron mobility. At the same time, it can also enhance the π–π stacking between molecules. Compared with PSCs containing dithiophene-based molecules, the PSCs containing these trithiophene NF-SMAs TPTTT-2F, *α*-IT and MeIC1 (Fig. 5) have improved PSC performance parameters, including V_{oc}, J_{sc} and FF[38, 44, 45]. PBDB-T:MeIC1 blended film has an area of 3.8 mm^2 as the active layer, and its device has obtained the best PCE of 12.58%, with a V_{oc} of 0.93 V, J_{sc} of 18.32 mA/cm^2 and FF of 74.1%. These results indicate that extending the conjugation length of the IDT core is an effective way to improve photovoltaic parameters and achieve high PCEs.

The asymmetric structures of 4,4,9,9-tetrakis(4-hexylphenyl)-4,9-dihydro-s-indaceno[1,2-b]thiophene[3,2-b]thiophenealt-[5,6-d]dithieno[3,2-b:2′,3′-d]thiophene (IDT8) core give full play to extended conjugation and asymmetric core advantages. This asymmetric structure can not only expand the spectral absorption and shift the LUMO energy level up but also increase the dipole moment and fine-tunes relevant parameters. Gao et al. designed and synthesized two asymmetrical small molecule acceptors (IDT6CN-M and IDT8CN-M) (Fig. 5). The pure film for IDT8CN-M and IDT6CN-M comparable absorption coefficient of 1.35 × 10^5 and 1.29 × 10^5 cm^{-1} with distinguishing maximum absorption wavelength values of 699 vs. 693 nm. It can be seen that IDT8CN-M has a long conjugation length and a large maximum absorption wavelength[43]. After using 0.5% DIO as a solvent additive and thermal annealing at 100 °C, the coherence length and domain purity are improved. In the end, the PCE of the device based on IDT8CN-M was further improved to 12.43%, mainly due to the increase in the J_{sc} value from 15.97 to 17.11 mA/cm^2, and the increase in the FF value from 76.1% to 78.9%. To further optimize the molecular structure and obtain a better balance between V_{oc} and J_{sc}, Li *et al.* synthesized three A-NF-SMAs (TTPTTT-IC, TTPTTT-2F and TTPTTT-4F) (TT-IC, TTPTTT-2F and TTPTTT-4F) (Fig. 5) by introducing three-terminal groups with different electron withdrawing properties and using an asymmetric TTPTTT building block as

the central core unit. For TTPTTT-4F, the addition of fluorinated 2-(3-oxo-2,3-inden-1-ydenne) malononitrile (IC) terminal groups will cause a red shift in light absorption and reduce the LUMO energy level. TTPTTT-4F also has improved electron mobility and intramolecular solid or intermolecular interactions[46]. PSCs based on fluorinated NF-SMAs showed significantly higher J_{sc} and FF than their non-fluorinated TTPTTT-IC counterparts. The device achieved a PCE of 12.05% with PBT1-C as polymer donor and TTPTTT-4F as acceptor, thanks to more coordinated performance parameters, especially the significant improvement in J_{sc}.

Compared with thiophene-based NF-SMA, selenophene-based NF-SMA has received much less attention, and the performance of the related device is also poor. To promote the absorption of non-fullerene acceptor small molecules, reduce their bandgap, and increase their LUMO energy level, Sun's research group designed an asymmetric small molecule acceptor SePT-IN by introducing a single-sided selenium atom into the core unit of the symmetric small molecule acceptor TPT-IN (Fig. 5)[47]. When blended with polymer donor PBT1-C (Fig. 4), the SePT-IN finally obtained 10.20% PCE higher than that of TPT-IN, mainly due to the significantly improved J_{sc}. Then, Li *et al*. designed and synthesized two selenophene-containing A-NF-SMAs SePTT-2F and SePTTT-2F (Fig. 5) with the same terminal group[48]. Moreover, Compared with SePTT-2F, SePTTT-2F has a larger conjugation area in the main chain, and SePTTT-2F exhibits a higher LUMO energy level and higher electron mobility. Both SePTTT-2F and SePTT-2F have similar band gaps and red-shifted absorption peaks. Pairing it with the polymer donor PBT1-C, the performance of PSCs based on SePTTT-2F reached an impressive PCE of 12.24% with an outstanding FF of 75.9%, which was much higher than that of PSCs based on SePTT-2F. Since the SePTTT-2F system has a higher and more balanced charge transfer than SePTT-2F, SePTTT-2F has more effective exciton dissociation and charge collection. Among selenophene-based NF-SMAs, this is the highest value reported in the literature.

Wang *et al*. and Gao *et al*. designed and synthesized A-NF-SMAs with the thienobenzodithiophene structure as the core TBDB-Na, TBDB-Ph, and a-BTTIC (Fig. 5)[49, 50]. The ultraviolet-visible absorption redshift of TBDB-Na relative to TBDB-Ph made the LUMO energy level decrease from −3.74 to −3.77 eV, while the J_{sc} of the device based on PTBD-BZ:TBDB-Na increase from 17.50 to 19.60 mA/cm^2. PTBD-BZ:TBDB-Na-based devices achieved a PCE_{max} of 12.47%, which is superior to that of the PTBD-BZ:TBDB-Ph-based devices (11.06%). The LUMO energy level of a-BTTIC is −3.83 eV, which is lower than TBDB-Na and TBDB-Ph, while its HOMO energy level is −5.45 eV, which is similar to that of TBDB-Na and TBDB-Ph. Therefore, the a-BTTIC has a very narrow bandgap, and the J_{sc} of the device based on PBDB-T:a-BTTIC blend film reaches up to 20.31 mA/cm^2, resulting in a high PCE of 13.60%. The high performance of these molecules is due to the appropriate energy level matching the donor, the excellent crystallinity of the active layer, and the balanced miscibility.

The electronegativity of nitrogen and sulfur atoms are 3.04 and 2.58, respectively. Compared with non-N-functionalized molecules in an asymmetric system, the introduction of nitrogen can further adjust the molecules' dipole moment. As shown in Fig. 6, the change of the sulfur atom to a nitrogen atom in the middle of the trithiophene unit determines the design of the dithieno[3,2-b:2',3'-d]pyrrole (DTP) unit. The ability to take advantage of sp^2 hybrid nitrogen is the most prominent feature of the DTP unit. Besides, the lone pair of electrons on the vertical π orbital can delocalize along the π orbital of the molecule. Extending the delocalized π-electron system can narrow the optical energy bandgap (E_g^{opt}) and strengthen the π–π stacking between molecules[51, 52]. PCEs of the device based on those relevant materials are all above 10%[53–60]. Gao *et al*. designed and synthesized N7IT (Fig. 6) by introducing nitrogen into the molecule[44]. It has a red-shifted absorption of more than 50 nm and an improved LUMO energy level compared to *α*-IT. These features provide N7IT-based PSCs higher V_{oc}, $J_{sc,}$ and PCE (13.8%) than *α*-IT. In addition, by combining electron-rich N and molecular conformational features, the molecule for N8IT and N7IT comparable dipole moment of 12 and 5 Debye. The high dipole moment of N8IT is the root cause of excessive crystallization and poor morphology of N8IT molecule. The device based on N8IT has relatively low J_{sc}, FF, and PCE (11.92%). To fully explore the influence of molecular conformation on molecular packing and aggregation characteristics, Yang *et al*. designed molecules with different numbers of thiophene extension rings and used S·O interactions to fine-tune the molecular conformation[53].

In contrast to C-type IPTT-2F, S-type IPT-2F and IPTTT-2F (Fig. 6) mixed membranes have fewer traps to avoid recombination, conducive to proper phase separation and formation of better active layer morphology. When using PBDB-T as a polymer donor, the PCEs of PSCs based on IPT-2F and IPTTT-2F were 14% and 12.3%, respectively, which were higher than those of PSCs based on C-type molecule IPTT-2F. Later, Yang *et al*. designed and synthesized four molecules with different aggregation characteristics IPT-4F, IPT-4Cl, IPTBO-4F, and IPTBO-4Cl (Fig. 6) by introducing different N-alkyl chains and terminal groups[54]. The inherent characteristics of larger Cl atoms and longer C–Cl bonds significantly extend the main chain's stacking area, thereby enhancing molecules' aggregation. In contrast, the larger BO chain exerts a more significant spatial shielding effect on the main chain's accumulation. Both IPT-4F and IPTBO-4Cl showed outstanding performance when blended with PM6. It is worth noting that the PCE_{max} of PM6:IPTBO-4Cl-based PSCs is 15%, which is slightly higher than that of 14.96% of PM6:IPT-4F-based PSCs. Considering the 2-ethylhexyl branch's significance, Ma *et al*. and Li *et al*. introduced the 2-ethylhexyl branch on the N atom while using different terminal electron-withdrawing groups to carefully adjust the energy level, absorption, crystallinity, and miscibility of molecules[55, 56]. Electron-withdrawing ability of TPIC, TPIC-4Cl, TPIC-4F, and TPIC-2Cl (Fig. 6) gradually increased when the atom type was introduced by the terminal group from 1 H to 4 Cl to 4 F, leading to a gradual decrease in LUMO energy level and V_{oc}. In the thin-film state, due to the relatively high ICT intensity and the unique atomic properties of Cl, the absorption of TPIC-4Cl has a significant redshift, and the maximum absorption peak is at 804 nm. Moreover, when blended with PM6, PM6:TPIC-4Cl-based film maintains the most comprehensive absorption range and the narrowest bandgap. Besides, the most suitable miscibility and the most favorable morphology resulted in balanced charge trans-

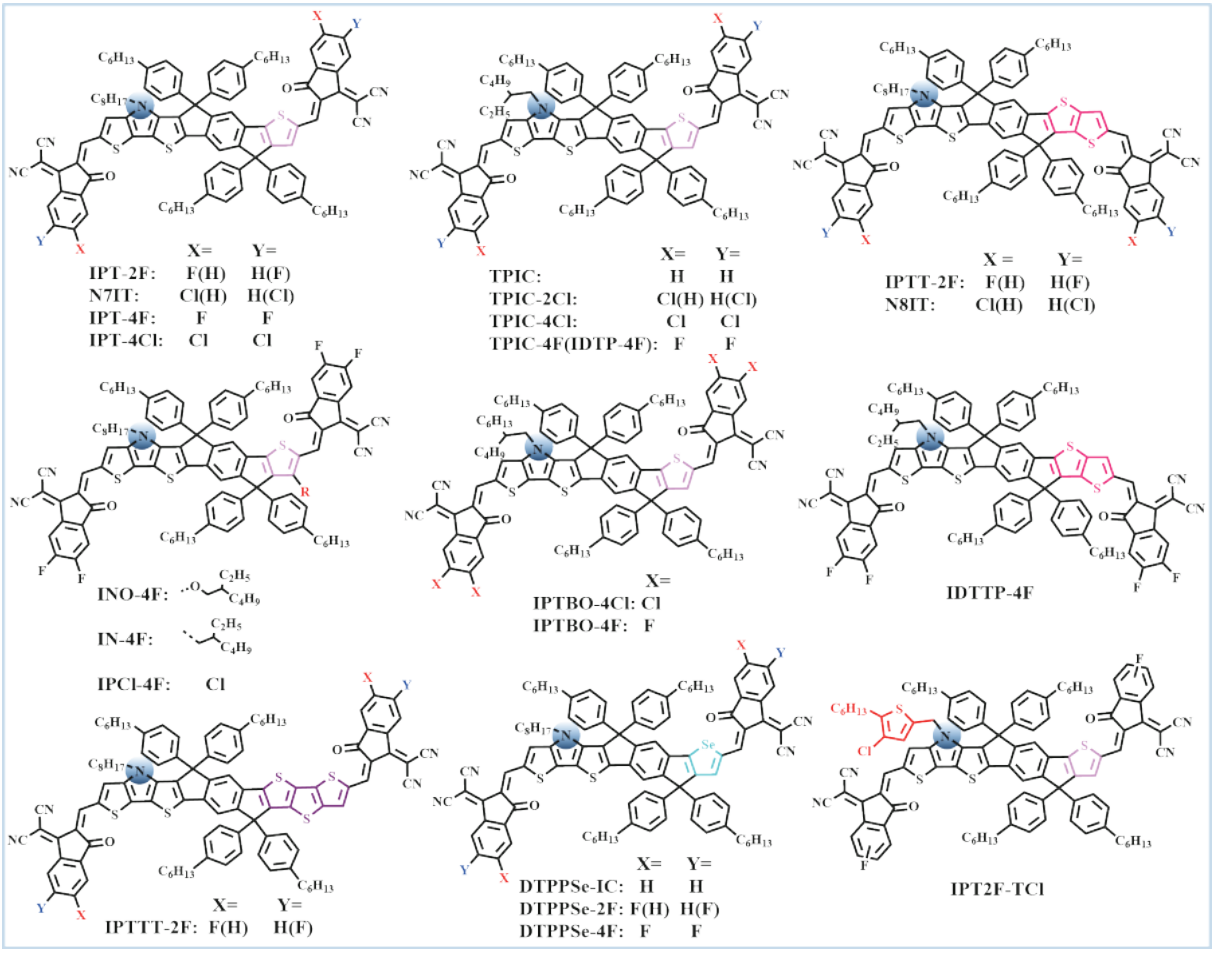

Fig. 6. Chemical structures of A–D–A asymmetric non-fullerene acceptors with nitrogen.

port, favorable phase separation, and effective exciton dissociation and extraction, so that the device based on PM6:TPIC-4Cl obtained the highest PCE of 15.31%.

After introducing the N atom, Cao *et al.* combined selenophene and DTP building blocks to prepare an asymmetric heptacyclic electron-donating core DTPPSe[57]. Compared to thiophene, selenophene has lower aromaticity, improved planarity, increased conjugation length, and lower E_g^{opt}. Meanwhile, selenide has a larger size and higher polarizability compared to sulfur. Therefore, selenene can induce the tendency of intermolecular Se–Se (chalcogen interaction) or selenium-aromatic interaction in the corresponding selenium-based NF-SMA. To systematically study the effect of fluorine-containing terminal groups on the photoelectric properties of selenophene-containing A-NF-SMAs, Cao *et al.* synthesized three new types of acceptors (DTPPSe-IC, DTPPSe-2F, and DTPPSe-4F) with IC unit, monofluorinated IC unit, or double fluorinated IC unit as showed in Fig. 6. With the increasing fluorine atoms, the E_g^{opt} of the three types of A-NF-SMAs gradually narrowed, LUMOs and HOMOs levels decreased, and the ultraviolet-visible absorption red shifted. These changes can promote the role of ICT and help to obtain better device performance. Simultaneously, great nano-fibrous and ordered phase-separated morphology are also conducive to charge transport and exciton dissociation. Therefore, the optimized devices for PBDB-T:DTPPSe-2F, PBDB-T:DTPPSe-IC and PBDB-T:DTPPSe-4F blends yield comparable PCEs of 13.76%, 9.88% and 12.03%. The PCE of the device based on PDBBT:DTPPSe-2F blend film is one of the highest values among A-NF-SMAs containing selenium in the literature.

Guo *et al.* and Luo *et al.* synthesized S-type seven-ring IDTP-4F and C-type eight-ring IDTTP-4F based on DTP and realized the adjustment of molecular conformation by changing the number of thiophenes on the right side (Fig. 6). IDTP-4F and IDTTP-4F both have good planar backbone conducive to intermolecular π–π packing[58, 59]. Both IDTP-4F and IDTTP-4F exhibit redshift absorption from solution to film, which indicates strong intermolecular interactions in the solid state. Compared with IDTP-4F, IDTTP-4F exhibits slight redshift absorption and a more pronounced shoulder peak. Three highly efficient polymer donors and two NF-SMAs IDTP-4F and IDTTP-4F are blended one-to-one to fabricate devices. The device performance test results show that the performance of the S-type IDTP-4F device is significantly better than that of the C-type IDTTP-4F device. The PCE based on PM7:IDTP-4F device reached 15.2%, a remarkable achievement among all binary systems. Zhang *et al.* designed a series of IPT-based A-NF-SMAs IN-4F, INO-4F, IPT-4F and IPCl-4F (Fig. 6) by adopting a corresponding side-chain of 2-ethylhexyl, 2-ethylhexyloxy, hydrogen or chloro onto thieno[2'',3'':5',6']-s-indaceno[2',1':4,5]dithieno[3,2-b:2′,3′-d]pyrrole (IPT) core. The charge density modulation of the IPT core was to systematically study its influence on the electronic structure, molecular stacking and photovoltaic performance of A-NF-SMAs[60]. According to the order of 2-ethylhexyloxy, 2-ethylhexyl, hydrogen, and chlorine, the electric traction ability of these four molecules gradu-

ally increases. The E_g^{opt} gradually shrinks and the LUMO energy level is reduced, making J_{sc} and V_{oc} achieve a good balance. When they were paired with polymer donor PM6, IPT-4F-based devices showed a high PCE of 14.62%. Compared with IPT-4F, PCEs of devices with INO-4F, IN-4F, or IPCl-4F as acceptors all decrease to different degrees.

Cao *et al*. introduced two-dimensional (2D) conjugated side chains into IPT core. They developed a 2D conjugated fused ring core semiconductor IPT2F-TCl (Fig. 6) as an electron acceptor for high-efficiency PSCs. The extended conjugate length in the ring core can optimize device performance[21]. IPT2F-TCl has a lower HOMO energy level of –5.59 eV and a wider absorption range, which leads to the asymmetric molecule IPT2F-TCl with a high PCE value of 13.74%. The 2D conjugated fused ring core asymmetric acceptor is expected to enhance interaction between molecules through a larger dipole moment so that PSCs have a higher FF and PCE.

In addition to changing the number of thiophene and introducing nitrogen and selenium atoms, the asymmetric design of the molecules can also be achieved by flipping the configuration for A–D–A-based non-fullerene acceptors. Luo *et al*. developed a novel NF-SMA ITCNTC (Fig. 7) with an asymmetric core by adjusting the configuration of thiophene[61]. Compared with the symmetrical molecule ITCPTC, the absorption spectrum of ITCNTC is blue-shifted, and the LUMO energy level rises. J71:ITCNTC-based devices have a PCE_{max} value of 8.52%, which is much lower than the 11.63% PCE_{max} value of J71:ITCPTC-based devices. The blue absorption shift and poor morphology of ITCNTC resulted in a sharp drop in both J_{sc} and FF, which led to a rapid decrease in PCE, although V_{oc} increased to some extent due to the rising LUMO level. This discovery confirmed that changing the direction of thiophene units to design asymmetric structures may not succeed sometimes.

Jiao *et al*. designed and synthesized an A–D–A typed acceptor CC10 with asymmetric donor units by introducing alkylbenzene units into CC5 (Fig. 7)[62]. The ground state dipole moments of CC5 and CC10 are 2.48 and 2.52 Debye, the excited state dipole moments of CC5 and CC10 are 2.37 and 6.80 Debye, the change in the dipole moment from the ground to the excited state for CC5 and CC10 is 0.11 and 7.97 Debye, respectively. The ground state dipole moment of the asymmetric molecule CC10 is slightly larger than that of CC5, which is conducive to enhancing the intermolecular interaction and intramolecular charge transfer characteristics. The stacking geometric configurations of CC5 dimer and CC10 dimer are shown in Fig. 8(b). CC5 dimer only exhibits one stacking form, while asymmetric CC10 dimer has three stacking forms. In addition, compared with the CC5 dimer, the CC10 dimer exhibits stronger intermolecular binding energy and stable geometric configuration, indicating that CC10 exhibits stronger π–π stacking and higher electron mobility in density functional theory (DFT). In contrast to symmetric molecule CC5, asymmetric molecule CC10 achieves better π–π stacking with a similar absorption range and energy level. Therefore, the PCE of CC10-based PSCs is as high as 11.78%, which is higher than that of CC5-based devices (6.91%). Wei Hu et al. synthesized N65-IC and N65-2FIC based on the naphthalene dithiophene core (Fig. 7). N65-2FIC composed of fused eight rings[63]. Compared with the S-NF-SMAs N66-IC and N66-2FIC with two six-ring bridges, their asymmetric constitutional isomers N65-IC and N65-2FIC with one six-ring bridge and one five-ring bridge both possessed red-shift absorption, better π–π stacking, and higher crystallinity. The LUMO energy levels of N66-IC and N65IC are –3.85 and –3.89 eV, respectively. The LUMO energy levels of N66-2FIC and N65-2FIC are –4.00 and –4.03 eV, respectively. The significant reduction of LUMO energy levels results in a narrow bandgap. PBDB-T-2F:N65-2FIC-based devices have a PCE_{max} value of 10.19%, which is three times higher than the PCE_{max} value of PBDB-T-2F:N66-2FIC-based devices (3.46%). PBDB-T:N65-IC-based devices have a PCE_{max} value of 9.03%, which is higher than the 5.45% PCE_{max} value of PBDB-T:N66-IC-based devices.

Among various core transformation engineering methods for designing asymmetric core units based on symmetrical analogs, the simplest method is to construct structural asymmetry by cutting off the side chains of the symmetric core. Many studies have been conducted on acceptors (ITOTC, ITUTC, ITUIC, IEPC, IOPC, IETC, IOTC, PhITBD, MeITBD, ITDI and CDTDI) that match to donor PBDB-T, and acceptors (PhITBD, TIDT-BT-R2, TIDT-BT-R6, ITBR, ITBRC and ITBC) match to donor PTB7-Th (Fig. 7). Zhang *et al*. synthesized three A–D–A type A-NF-SMAs (ITOTC, ITUTC and ITUIC)[64]. There are only two side chains in the indenothiophene unit of ITUIC, limiting the solubility and crystallinity of the corresponding NF-SMAs, which lead to poor miscibility with PBDB-T. According to the absorption onsets of the acceptors in thin films, optical band gaps of ITOTC, ITUTC and ITUIC are calculated to be 1.61, 1.60 and 1.64 eV, respectively. Under the condition that the polymer donor is PBDB-T, compared with the symmetric molecule ITIC, the asymmetric molecule ITUIC has less absorption complementarity with the donor, so the band gap between ITUIC and the donor is wider. Therefore, under the same device fabricating conditions, ITUIC-based devices show worse device performance than ITIC-based devices. The optimized devices for PBDB-T:ITUIC and PBDB-T:ITIC blends yield comparable PCEs of 6.45% and 8.66%[65]. Similar to ITUIC, the ITUTC-based PSCs (7.68%) and the ITUTC-based PSCs (8.35%) all showed reduced PCEs than that of symmetric ITCPTC-based PSCs (11.92%)[95]. By shearing the side chain of the central core of the symmetrical IEIC molecule, Kang *et al*. synthesized four different A-NF-SMAs (IOTC, IETC, IOPC, and IEPC) to investigate the effect of different terminal acceptor units on photovoltaic properties[66, 67]. Compared with the IOPC and IEPC, IOTC and IETC both exhibit remarkable red-shifted absorption, smaller E_g^{opt}, higher hole and electron mobility, which is consistent with that the enhanced electron-withdrawing ability from IC to 2-(6-oxo-5,6-dihydro-4H-cyclopenta[c]thiophen-4-ylidene)malononitrile (TC). Hence, with PBDB-T as the donor, the best performance binary devices based on IOTC and IETC exhibited PCEs of 7.94% and 7.40%, which are higher than that of binary devices based on IOPC and IEPC (4.86% and 5.26%). Kim *et al*. designed a new type of A-NF-SMAs (PhITBD) with an indole thiophene nucleus[69]. The twist angle between the linearly connected thiophene and the end group of PhITBD is 22°, which is shown in Fig. 8(c). It was found that the asymmetric molecule PhITBD has a twisted structure, while the symmetrical molecule IDT-2BM has a trapezoidal shape structure. As shown in Fig. 8(b), the cal-

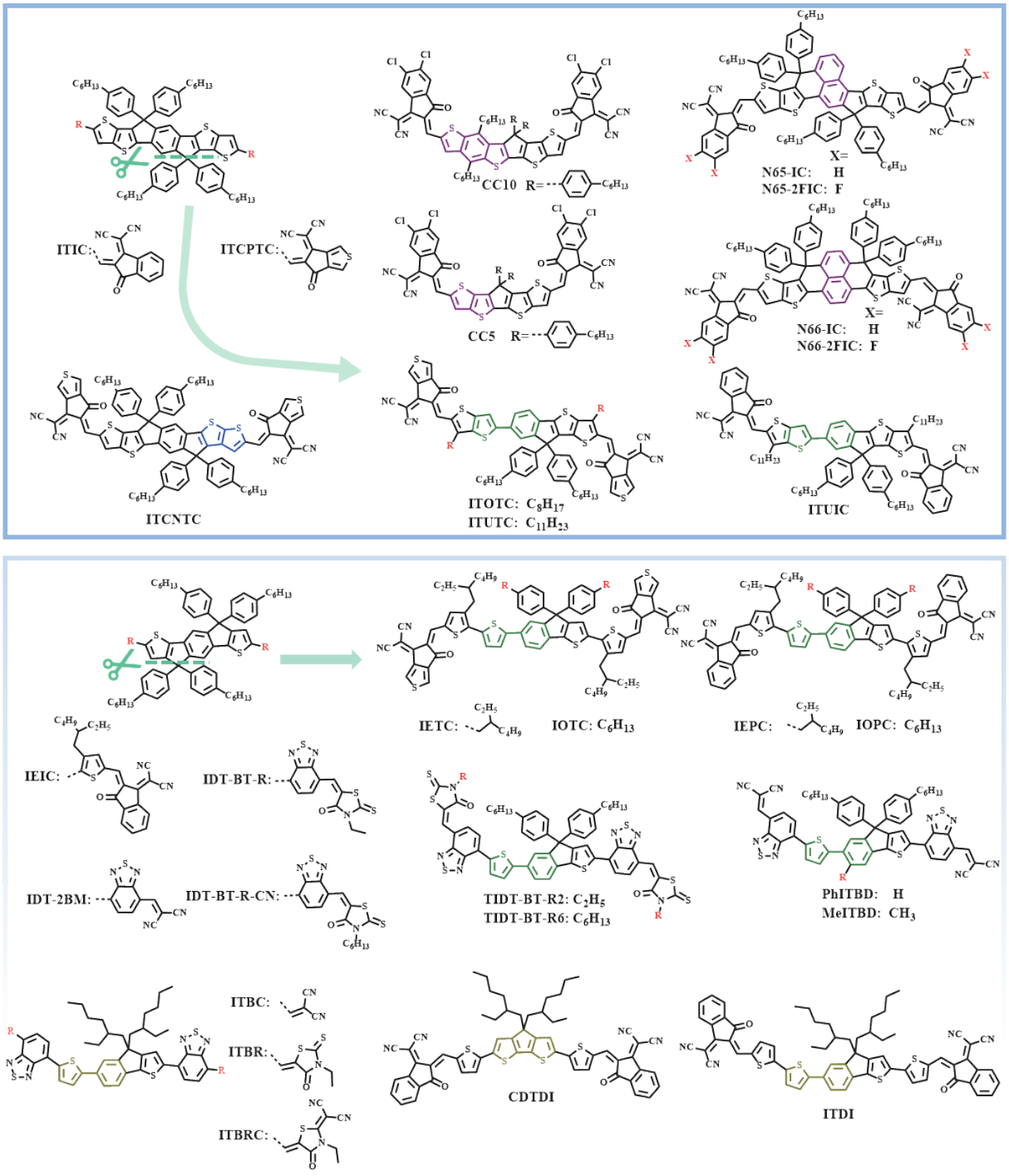

Fig. 7. Chemical structures of other asymmetric non-fullerene acceptors based on the A–D–A structure and the molecules that are associated.

culated LUMO energy levels of IDT-2BM and PhITBD are –3.65 and –3.69 eV, and the calculated HOMO energy levels of IDT-2BM and PhITBD are –5.56 and –5.74 eV, respectively. The asymmetric molecule PhITBD has a lower HOMO energy level and a larger calculated band gap energy than IDT-2BM. The asymmetric structure of PhITBD enhances internal morphology and the effective regulation of energy levels. Compared with symmetrical molecule IDT-2BM, the film formed by blending PhITBD and donor PTB7-Th has higher molar absorption, more balanced charge transport and well-defined nanophase separation. Due to effective morphology control and absorption enhancement, PTB7-Th:PhITBD-based devices have a PCE_{max} value of 6.57%, which is higher than the PCE_{max} value of PTB7-Th:IDT-2BM-based devices (3.97%). It reveals that the molecular cutting strategy has a specific practical meaning for the design of asymmetric cores. Jeong *et al.* synthesized the asymmetric molecule MeITBD by introducing a methyl substituent at the 7-position of indenothiophene into the molecule PhITBD[97]. The methyl substitution makes MeITBD have a more twisted structure than PhITBD, which reduces the self-association capability of whole molecules, resulting in better miscibility between MeITBD and PBDB-T, thus forming a smoother surface morphology. PBDB-T:Me-ITBD-based devices have a PCE_{max} value of 5.75%, which is higher than the 1.78% PCE_{max} value of PBDB-T:Ph-ITBD-based devices. This is attributed to the side-group engineering by placing a methyl group on the bay side of PhITBD, forming an acceptable form that is conducive to the performance of PSCs.

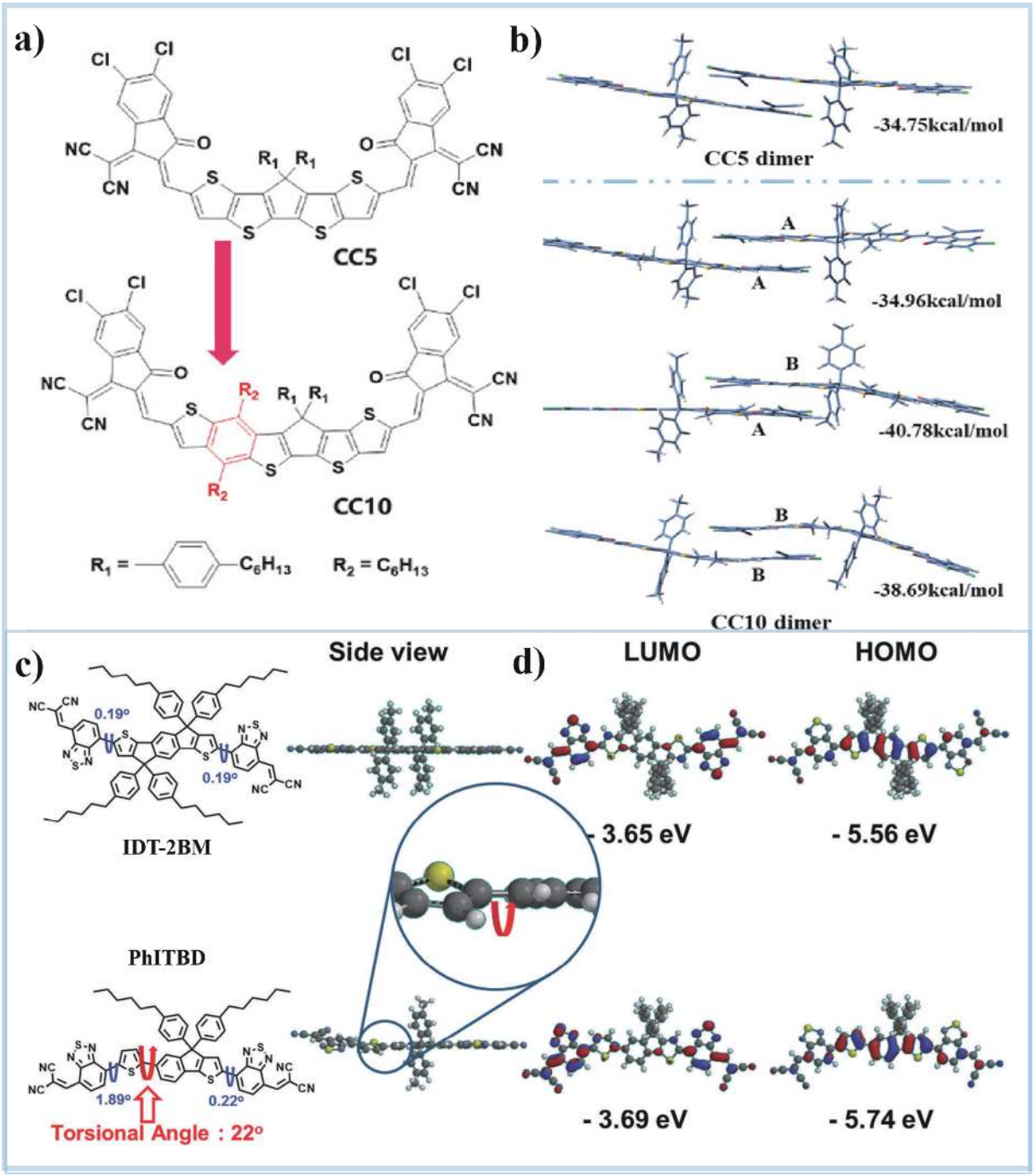

Fig. 8. (a) Chemical structure of CC5 and CC10. (b) Optimized geometries and the corresponding intermolecular binding energies by DFT calculations of CC5 and CC10 dimers. Reproduced with the permission of Ref. [62]. (c) The molecular structures, (d) DFT calculated geometries (side view), and the HOMO/LUMO (top view) structures of IDT-2BM and PhITBD. Reproduced with the permission of Ref. [69].

The molecules (TIDT-BT-R2 and TIDT-BT-R6) with the same molecular core and different terminal groups to PhITBD were reported by Bai *et al.*[68]. TIDT-BT-R2 and TIDT-BT-R6, as compared to the symmetrical molecules (IDT-BT-R and IDT-BT-R-CN), both have a reduced fused-ring central core thiophene-indenothiophene (TIDT)[68, 70, 71]. Although the large side chains of the sp^3 hybridization of central core TIDT are reduced, TIDT-BT-R2 and TIDT-BT-R6 (Fig. 7) can still maintain close molecular packing. On one hand, this TIDT core can obtain a higher molar extinction coefficient, more substantial thermal stability, and better-regulated energy levels than the fully fused-ring central core IDT. On the other hand, TIDT-BT-R2 has good crystallinity and high carrier mobility due to the short-chain length of the substituents of terminal groups. Therefore, PTB7-Th:TIDT-BT-R2-based devices have a PCE_{max} value of 8.7%, which is higher than that of PTB7-Th:IDT-BT-R2-based devices (8.3%). However, the longer the chain length of the substituents, the weaker the effect of the asymmetric core in reducing molecular self-association. Therefore, the molecular self-association ability of TIDT-BT-R6 is stronger than that of TIDT-BT-R2. The optimized devices for PTB7-Th:TIDT-BT-R6 and PTB7-Th:IDT-BT-R-CN blends yield comparable PCEs of 5.6% and 5.7%. The above results indicate that reducing the fusion of core units is an effective strategy to

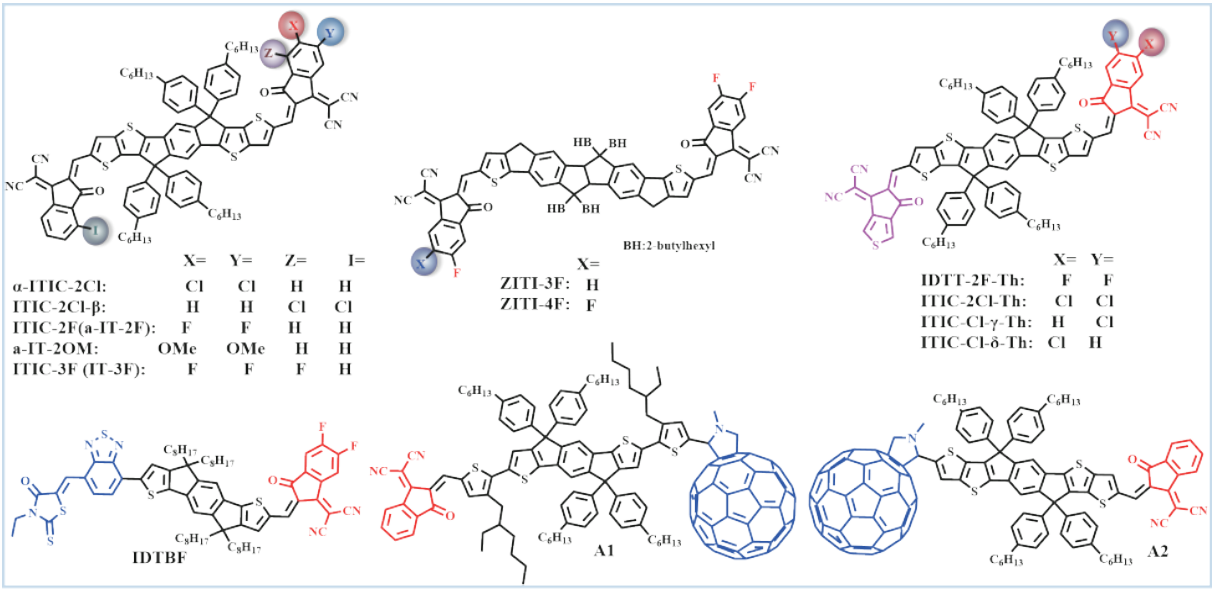

Fig. 9. The chemical structures of asymmetric non-fullerene acceptors are based on asymmetric terminal groups and their molecules.

achieve high-performance functions. The PCEs of other asymmetric core molecules (ITBC 4.26%, ITBRC 6.27%, ITBR 7.49%, ITDI 8.0% and CDTDI 2.75%) were reported earlier by Tang *et al.* and Kang *et al.*[29, 72]. The bandgaps and energy levels of these A-NF-SMAs (ITBC, ITBRC, ITBR, ITDI and CDTDI) can be easily adjusted by changing terminal groups' electron-withdrawing ability. Besides, the highest PCE of these acceptors-based PSCs can achieve up to 8%, indicating that small molecules with asymmetric indenothiophene as the core can become a new type of non-fullerene acceptor for PSCs.

3.2. A-NF-SMAs with asymmetric terminal groups

Different terminal groups can induce the permanent dipole moment of A–D–A typed A-NF-SMAs molecules to regulate intermolecular interactions, leading to a more diverse aggregation tendency of the molecules affecting the π–π stacking, crystallization characteristics, and final photovoltaic performance[73]. Simultaneously, combining two-terminal groups with different polarities in a single molecule can fine-tune the absorption and energy level, making the asymmetric A1–D–A2 strategy for energy level tuning possible[74, 75].

ITIC is a typical NF-SMA with the advantages of easy synthesis, strong absorption in the visible light region, adjustable energy level and good stability. Adjusting terminal group substituents is a recent research hotspot in asymmetric terminal group strategy. Lai *et al.*, Aldrich *et al.*, Li *et al.*, and Gao *et al.* used ITIC as the main body and changed the terminal substituents (chlorine, fluorine, hydrogen, and methoxy) to synthesize four different asymmetric molecules *α*-ITIC-2Cl, ITIC-2F (its structure is the same as a-IT-2F), ITIC-3F (its structure is the same as IT-3F), and a-IT-2OM (Fig. 9)[76–79]. The position of the chlorine substitution of the asymmetric molecule *α*-ITIC-2Cl was changed, and a completely different crystal structure of the symmetric molecule ITIC-2Cl-*β* (Fig. 9) was constructed. Compared with the linear stacking structure of the symmetric molecule ITIC-2Cl-*β*, the three-dimensional interpenetrating network structure of the asymmetric molecule *α*-ITIC-2Cl changes the stacking method of molecules, enhances the interaction between molecules, and shortens the π–π stacking distance. The molecules ITIC-2Cl-*β* and *α*-ITIC-2Cl showed comparable electron mobilities of 1.1×10^{-4} and 2.9×10^{-4} cm^2/(V·s) hole mobilities of 2.4×10^{-4} vs. 4.2×10^{-4} cm^2/(V·s), with hole/electron mobility ratios of 1.4 and 2.2, respectively. Higher electron mobilities, hole mobilities, and balanced mobility ratios indicate faster charge transfer in the *α*-ITIC-2Cl based devices[76]. Higher charge mobility can be realized in the *α*-ITIC-2Cl compared with ITIC-2Cl-*β*, leading to a higher J_{sc} in the PSCs. Finally, a high PCE of 12.2% is obtained by *α*-ITIC-2Cl, which is 10% higher than that of ITIC-2Cl-*β*. Asymmetric chlorine substitution is beneficial to increase charge mobility, thereby promoting device efficiency. Asymmetric chlorine substitution improves the stacking method between molecules, which helps increase the charge mobility, thereby promoting the increase of the PCEs of PSCs. Both ITIC-2F and ITIC-3F (Fig. 9) are A-NF-SMAs with one fluorinated terminal group and one non-fluorinated terminal group. Compared with molecules with symmetrical A–D–A structures, ITIC-2F and ITIC-3F increase molecular order and electron transport in informative ways. With PBDB-TF (its structure is the same as PM6) as the donor, the performance binary devices based on ITIC-2F and ITIC-3F exhibited PCEs of 10.38% and 11.44%, respectively[77]. a-IT-2F, which is synthesized by Li *et al.*, has the same molecular structure as the ITIC-2F (Fig. 9) synthesized by Aldrich *et al.*[77, 78]. The ITIC-3F has the same molecular structure as the IT-3F (Fig. 9) synthesized by Gao *et al.*[77, 79]. When PBDB-T or PBDB-TF (its structure is the same as PM6) was used as the donor, the performance of binary devices based on a-IT-2F (its structure is the same as IT-IC-2F) and IT-3F (its structure is the same as ITIC-3F) exhibited PCEs of 10.28% and 13.83%, respectively[78, 79]. a-IT-2OM has methoxy substitutions different from the F substitutions of a-IT-2F (Fig. 9). The methoxy group causes a stronger terminal dipole moment, effectively regulating the molecular binding energy, crystalline properties, and microscopic morphology of the blended films, promoting close molecular packing and effective charge transfer. The improved charge transfer characteristics support the improved device performance of a-IT-2OM (PCE_{max} = 12.07%, FF = 71.52%, J_{sc} = 18.11 mA/cm^2, V_{oc} = 0.93 V), which are better than those of a-

IT-2F (PCE_{max} = 10.28%, FF = 68.84 %, J_{sc} = 0.78 mA/cm^2, V_{oc} = 0.78 V).

Ye *et al*. synthesized an A-NF-SMA, named IDTT-2F-Th[80]. Lai *et al.* synthesized three chlorine-substituted asymmetric non-fullerene acceptors, named ITIC-Cl-δ-Th, ITIC-Cl-γ-Th, and ITIC-2Cl–Th (Fig. 9)[81]. One terminal group of this kind of molecule is the fluorinated or chlorinated IC group, and the other is the 2-(6-oxo-5,6-dihydro-4H-cyclopenta[c]thiophen-4-ylidene)malononitrile (TIC) group[80, 81]. Since IDTT-2F-Th has two different terminal groups, the ultraviolet-visible maximum absorption wavelength (731 nm) of the film of the asymmetric molecule IDTT-2F-Th is red-shifted a bit compared with that of the symmetric molecule ITCPTC (725 nm). Simultaneously, the IDTT-Th HOMO energy level of 2F-Th is higher than that of ITCPTC, and the bandgap (1.69 eV) of IDTT-2F-Th energy level is smaller than that of ITCPTC (1.74 eV). Although the asymmetry structure caused by two different terminal groups leads to a slight decrease in the order of IDTT-2F-Th molecular stacking, the carrier mobility of IDTT-2F-Th:PBT1-C-2Cl mixture can still reach 53% the above. Ultimately, the PBT1-C-2Cl:IDTT-2F-Th device can obtain a PCE of 12.01%, higher than the 10.9% of the PBT1-C-2Cl:ITCPTC device. Among the three molecules of ITIC-2Cl-Th, ITIC-Cl-γ-Th and ITIC-Cl-δ-Th, ITIC-2Cl-Th has the largest number of chlorine atoms, the lowest LUMO, and the lowest *V*oc, which is the reason for hindering the improvement of PCE. Comparing to the two chlorines ITIC-2Cl-Th and single chlorine at the δ-position of ITIC-Cl-δ-Th, the single chlorine at the γ-position of the ITIC-Cl-γ-Th terminal group can lead to the best molecule flatness and the lowest dimer energy, which is conducive to the charge transfer between molecules. Simultaneously, the monochlorination of γ-position helps to improve the mobility of electrons and holes. Simultaneously, the inverse structure device PBDB-TF:ITIC-Cl-γ-Th achieves the most effective exciton dissociation and the weakest bimolecular recombination so that the ITIC-Cl-γ-Th-based best device obtains an excellent PCE of 12.25%.

With dithienocy-clopentaindenoindene (ZIT) as the core, Zhang *et al*., through one-pot Knoevenagel reaction, synthesized ZITI-m, a mixture of A-NF-SMA ZITI-3F and S-NF-SMA ZITI-4F (Fig. 9)[82]. Compared with ZITI-3F and ZITI-4F, the one-pot synthesis of mixed material ZITI-m is easier. In the film, ZITI-m shows a higher molar extinction coefficient and a more red-shifted ultraviolet-visible absorption than ZITI-3F and ZITI-4F, resulting in ZITI-m forming the narrowest E_g^{opt} (1.48 eV). Using J71 as the donor, the optimized devices of J71:ZITI-3F and J71:ZITI-4F produced 12.97% and 13.02% efficiencies. In contrast, J71:ZITI-m-based PSC shows a very high PCE of 13.65%, which shows that compositing asymmetric molecular with symmetric molecular has great potential in developing PSCs. Duan et al. combined two different terminal groups, rhodanine-flanked benzo[c][1,2,5]thiadiazole (BR) and 2-(5,6-difluoro-3-oxo-2),3-dihydro-1H-inden-1-ylidene) malononitrile (IM2F), connected to IDT core, constructing a new A-NF-SMA IDTBF (Fig. 9)[83]. The device's hole/electron mobility ratio (1.19) based on polymer donor PM6 and asymmetric molecule IDTBF is close to 1, ensuring effective charge transfer and collection. PM6:IDTBF devices show a satisfactory photocurrent response in the 350 to 750 nm range, and devices based on polymer donor PM6 and IDTBF show promising PCE of 10.43%. Zhao *et al*. designed and synthesized two fullerene/non-fullerene hybrids as small molecule acceptors A1 and A2 (Fig. 9) for PSCs[84]. These two hybrids introduce fused-ring IDT and IDTT as the core, respectively, and connect to the linear conjugate unit of C60, aiming to combine the photoelectric properties of PCBM and ITIC. A1 and A2 show UV–Vis absorption in 300–500 and 500–800 nm, respectively. The absorption in the high-energy region can be attributed to fullerenes, while the absorption in the low-energy region comes from intramolecular interaction between the inner core and IDM. Acceptor A2 combines the characteristics of PCBM and ITIC. This combination increased the PCE to 4.52% when the device's V_{oc} (J71 as donor) is close to 1.0 V.

These great performances of PSCs based on molecules with asymmetric terminal groups reveal that it is meaningful to adjust the molecular polarity and stack morphology through asymmetric modification of the terminal groups.

3.3. A-NF-SMAs with asymmetric side chains

Side-chain engineering is crucial for device performance, which can alter crystallinity, miscibility, and intermolecular interactions. A suitable side chain can endow the acceptor molecules with good solubility so that the blended film has an appropriate nanoscale phase separation. It can also prevent small molecules from forming hydrogen aggregates and increase the charge transport rate.

Alkyl and alkaryl groups are generally used as side chains of A-NF-SMAs. Compared to acceptors with alkyl aryl groups, alkyl-substituted acceptor molecules have a shorter π–π stacking distance than alkyl aryl groups. Feng *et al*. synthesized two A-NF-SMAs IDT-OB and IDTT-OB (Fig. 10) through side-chain engineering[85, 86]. The introduction of asymmetric side chains in the asymmetric molecule IDT-OB increases the solubility of the acceptor molecule and forms stereoisomers, effectively reducing the crystallinity. Compared with symmetrical molecules IDT-2O and IDT-2B, IDT-OB (Fig. 10) obtains a closer packing between molecules in a dislocation manner and forms a better phase separation when mixed with PBDB-T. As expected, the IDT-OB-based PSCs (10.12%) showed higher PCE than those of IDT-2O-based PSCs (9.68%) and IDT-2B-based PSCs (6.42%). When the central core of the IDT-OB molecule extended from the five-heterocyclic IDT core to the seven-heterocyclic indacenodithieno[3,2-b]thiophene (IDTT) core, while the side chain remains unchanged, a new asymmetric molecule IDTT-OB was synthesized. The extended conjugation length makes IDTT-OB have wider UV–Vis absorption and higher HOMO energy level than IDT-OB. Therefore, when mixed with PBDB-T, the blended film shows strong molecular packing and high crystallization behavior, with strong plane orientation. The optimized devices for PBDB-T:IDTT-OB and PBDB-T:IDTT-OB blends yield comparable PCEs of 11.19% and 10.12%.

Lee *et al*. synthesized A-D-A-type side-chain asymmetric small molecules p-IO1 and o-IO1 (Fig. 10)[87]. By introducing alkoxy groups to form asymmetry to manipulate photoelectron properties and intermolecular organization, o-IO1 and p-IO1 acceptors obtained better photovoltaic performance than the symmetrical molecules o-IO2 and p-IO2. Simultaneously, the two A-NF-SMAs (o-IO1 and p-IO1) and donor PTB7-Th formed a suitable bandgap and favorable PSC photoactive layer morphology. Hence, PTB7-Th:o-IO1-based PSCs (26.3 mA/cm^2) and PTB7-Th:p-IO1-based PSCs (22.3 mA/cm^2)

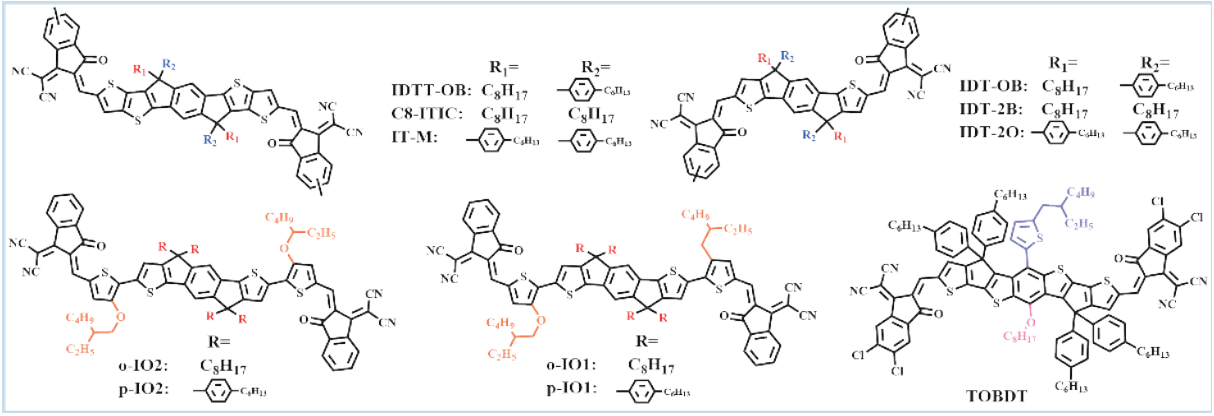

Fig. 10. Chemical structure of asymmetric non-fullerene acceptors based on asymmetric branched chains and the molecules associated with them.

all have high J_{sc} and low energy loss of about 0.54 eV. The PSCs based on PTB7-Th:o-IO1 and PTB7-Th:p-IO1 showed PCEs (13.1% and 10.8%) higher than those of PSCs based on PTB7-Th:o-IO2 and PTB7-Th:p-IO2 (10.8% and 9.30%).

Chen *et al.* designed an A-NF-SMA TOBDT (Fig. 10) based on the benzo[1,2-b:4,5-b']dithiophene (BDT) fused central core with asymmetrical alkoxy and thienyl side chains[88]. The molecular dipole moment generated by the asymmetric side chain and the S–S interaction of the thienyl unit all leads to the enhancement of the intermolecular interaction. The alkoxy group's electron-donating property can help narrow the bandgap by improving the HOMO. Moreover, the other side chain can be used to precisely adjust the energy levels. As a result, TOBDT shows a low optical band gap of 1.41 eV and a suitable energy level, matching the donor PM6 well. The best binary PSCs based on PM6:TOBDT showed PCE of 11.3% (J_{sc} = 18.7 mA/cm^2, V_{oc} = 0.89 V, FF = 0.68).

It can be seen that the introduction of asymmetric side chains can increase the solubility of acceptor molecules, make the acceptor molecules densely packed in a dislocation manner, and form good phase separation and good device performance.

Table 1 covers the performance parameters of the acceptor–donor–acceptor (A–D–A) typed A-NF-PSCs.

4. Asymmetric non-fullerene acceptors based on A–D–A–D–A structures

A molecule with an A–D–A–D–A structure as the main body has two donor units and three acceptor units, which will cause this type of molecule to have a wider ultraviolet-visible absorption range than the A–D–A type structure. A–D–A–D–A type molecule has more donor units and acceptor units than the A–D–A type molecule, which can provide more frontier molecular orbitals to receive electrons from excited donors[89]. Moreover, as the most popular non-fullerene acceptor molecule at present, Y6 has a broad application prospect. Therefore, the following content (1) summarizes a series of adjustments and designs of Y6 by scientific research scholars so far; (2) discusses the advantages of asymmetric small molecules in terms of charge transfer, molecular energy levels, and active layer accumulation morphology; (3) records the device performance parameters of subsequent optimization-related devices.

4.1. A-NF-SMAs with asymmetric cores

Imitating the design idea of A–D–A molecules, Cai *et al.* designed and synthesized two new Y-series non-fullerene acceptors Y21 and Y22 (Fig. 11), with asymmetric cores and used them in the study of PSCs[93, 94]. Both acceptors have good solubility, strong UV–Vis absorption, and good molecular stacking. Due to the nanofilament morphology of the active layer after mild thermal annealing, PM6:Y21/Y22-based devices' PCE_{max} with inverted structure is up to 15.4%, with a J_{sc} over 24 mA/cm^2. Two new A1–D–A2–D–A1 typed Y-series A-NF-SMAs (c-type BDTP-4F and s-type BTDTP-4F), and two new A–D–A typed A-NF-SMAs (c-type IDTTP-4F and s-type IDTP-4F), were designed and synthesized by Luo *et al.* (Fig. 11)[59]. The PCE of BDTP-4F based PSCs with PM6 as the donor was 15.24%, significantly higher than that of BTDTP-4F based devices (13.12%). For the A–D–A structure, IDTP-4F with the s-shaped conformation is better than IDTTP-4F with the c-shaped conformation. At the same time, the better-performing binary mixture has similar morphological characteristics. Zhang *et al.* designed and synthesized a new type of asymmetric molecule TB-4Cl (Fig. 11)[92]. This molecule obtains a 1.98 Debye dipole moment by changing the Y6 (dipole moment = 1.07 Debye) structure to TB-4Cl, further enhancing the intermolecular dipole-dipole interaction. At the same time, TB-4Cl has more dipole moments along with the molecular framework. With a more balanced positive and negative potential distribution on the terminal group, a positive potential is conducive to charge transfer and J-aggregation. As shown in Fig. 12(a), TB-4Cl contains dihedral angles of 0.74° and 0.61°, so TB-4Cl has a planar structure that is conducive to π–π packing and electron mobility. Due to the asymmetric structure, TB-4Cl has two anti-parallel packing methods (TB-4Cl-1T1, TB-4Cl-2T2) (Figs. 12(c) and 12(d)), while Y6 has only one type. Under DFT calculations, the stacking distance of TB-4Cl-2T2 and TB-4Cl-1T1 are 11.03 and 13.99 Å, respectively, which is longer than that of the Y6 dimer. Compared with the Y6 dimer, TB-4Cl-2T2 and TB-4Cl-1T1 bind stronger, which is conducive to limiting the thermal movement of molecules and improving stability. The binding energy of TB-4Cl and the donor is greater than the binding energy of Y6 and the donor, so the binding of TB-4Cl and the donor is tighter, and the active layer is more stable. Its superior thermal stability makes PM6:TB-4Cl-based devices more efficient without

Table 1. Device parameters for A–D–A typed A-NF-SMA PSCs.

A-NF-SMA	E_g^{opt} (eV)	HOMO/LUMO (eV)	Donor	V_{oc} (V)	J_{sc} (mA/cm^2)	FF (%)	PCE_{max} (%)	Ref.
IPT2F-TCl	1.48	–5.59/–4.00	PBDB-T	0.860	20.59	77.51	13.74	[21]
TPTT-IC	1.63	–5.78/–3.95	PBT1-C	0.960	15.60	70.00	10.50	[37]
TPTT-2F	1.58	–5.75/–4.04	PBT1-C	0.881	15.82	73.00	10.17	[38]
TPTTT-2F	1.56	–5.69/–4.01	PBT1-C	0.916	17.63	74.50	12.03	[38]
T-TT	1.64	–5.43/–3.47	PM6	0.966	16.00	62.70	9.70	[39]
T-TT-4F	1.58	–5.44/–3.51	PM6	0.859	18.48	66.10	10.49	[39]
T-TT-4Cl	1.53	–5.48/–3.59	PM6	0.813	19.00	65.70	10.16	[39]
IDT6CN-M	1.63	–5.62/–3.90	PBDB-T	0.924	15.97	76.10	11.23	[40]
IDT8CN-M	1.58	–5.54/–3.91	PBDB-T	0.920	17.11	78.90	12.43	[40]
TPTT-T-2F	1.54	–5.60/–4.00	PBT1-C	0.915	18.50	75.10	12.71	[41]
IDT6CN	1.63	–5.68/–3.97	PBDB-T	0.830	15.14	73.77	9.27	[42]
IDT6CN-Th	1.61	–5.71/–4.01	PBDB-T	0.810	16.75	76.72	10.41	[42]
IDT6CN-M	1.65	–5.60/–3.87	PBDB-T	0.910	16.02	76.83	11.20	[42]
IDT6CN-TM	1.60	–5.70/–3.96	PM6	0.953	17.40	74.70	12.40	[43]
IDT6CN-4F	1.58	–5.78/–4.12	PM6	0.859	18.34	69.10	10.88	[43]
α-IT	1.54	–5.65/–3.99	PM6	0.907	16.60	76.20	11.46	[44]
N7IT	1.42	–5.47/–3.93	PM6	0.932	21.04	70.50	13.82	[44]
N8IT	1.42	–5.41/–3.90	PM6	0.943	18.53	68.20	11.92	[44]
MeIC1	1.54	–5.59/–3.89	PBDB-T	0.927	18.32	74.10	12.58	[45]
TTPTTT-IC	1.60	–5.64/–3.87	PBT1-C	0.996	12.47	63.70	7.91	[46]
TTPTTT-2F	1.54	–5.67/–4.04	PBT1-C	0.920	16.78	73.60	11.52	[46]
TTPTTT-4F	1.52	–5.69/–4.12	PBT1-C	0.863	19.36	72.10	12.05	[46]
SePT-IN	1.54	–5.77/–4.00	PBT1-C	0.850	16.37	73.30	10.20	[47]
SePTT-2F	1.50	–5.71/–4.00	PBT1-C	0.830	17.51	75.00	10.90	[48]
SePTTT-2F	1.50	–5.66/–3.97	PBT1-C	0.895	18.02	75.90	12.24	[48]
			PBDT-BZ	0.926	9.93	43.90	4.04	
TBDB-Ph	1.46	–5.44/–3.74	PTBD-BZ	0.925	18.13	65.90	11.06	[49]
			PDTBDT-BZ	0.913	13.41	51.80	6.20	
			PBDT-BZ	0.905	13.14	53.20	6.32	
TBDB-Na	1.41	–5.45/–3.77	PTBD-BZ	0.906	19.61	70.20	12.47	[49]
			PDTBDT-BZ	0.879	11.24	54.40	5.38	
a-BTTIC	1.43	–5.45/–3.83	PBDB-T	0.904	20.31	74.00	13.60	[50]
IPT-2F	1.44	–5.51/–3.96	PBDB-T	0.860	22.40	72.40	14.00	[53]
IPTT-2F	1.42	–5.46/–4.04	PBDB-T	0.874	19.70	66.20	11.40	[53]
IPTTT-2F	1.43	–5.40/–4.07	PBDB-T	0.894	20.00	69.30	12.30	[53]
IPT-4F	1.42	–5.57/–4.08	PM6	0.914	22.08	74.15	14.96	[54]
IPTBO-4F	1.41	–5.57/–4.07	PM6	0.917	22.08	72.45	14.67	[54]
IPT-4Cl	1.39	–5.58/–4.11	PM6	0.883	23.18	70.37	14.40	[54]
IPTBO-4Cl	1.39	–5.64/–4.08	PM6	0.893	23.15	72.57	15.00	[54]
TPIC	–	–	PM7	1.003	18.51	71.10	13.20	[55]
TPIC-4F	–	–	PM7	0.901	22.35	74.20	14.90	[55]
TPIC-4Cl	–	–	PM7	0.885	22.89	75.70	15.40	[55]
TPIC	1.50	–5.30/–3.85	PM7	1.002	18.77	70.90	13.33	[56]
TPIC-2Cl	1.45	–5.36/–3.92	PM7	0.941	21.37	72.20	14.53	[56]
TPIC-4Cl	1.40	–5.35/–3.97	PM7	0.881	23.03	75.50	15.31	[56]
DTPPSe-IC	1.46	–5.38/–3.84	PBDB-T	0.900	17.32	63.36	9.88	[57]
DTPPSe-2F	1.40	–5.52/–4.05	PBDB-T	0.840	22.16	73.70	13.76	[57]
DTPPSe-4F	1.39	–5.53/–4.10	PBDB-T	0.780	21.18	72.84	12.03	[57]
			PM6	0.871	22.30	73.40	14.30	
IDTP-4F	–	–5.54/–3.98	S1	0.892	22.40	73.20	14.60	[58]
			PM7	0.903	22.50	74.60	15.20	
			PM6	0.874	20.50	70.30	12.60	
IDTTP-4F	–	–5.53/–3.97	S1	0.897	21.40	70.20	13.50	[58]
			PM7	0.908	21.20	71.60	13.80	
IN-4F	1.45	–5.59/–3.94	PM6	0.920	19.50	69.65	12.50	[60]
INO-4F	1.46	–5.64/–3.93	PM6	0.930	20.46	71.95	13.69	[60]
IPT-4F	1.41	–5.56/–4.05	PM6	0.880	22.15	75.01	14.62	[60]
IPCl-4F	1.39	–5.60/–4.08	PM6	0.830	21.18	61.38	10.79	[60]
ITCNTC	1.68	–5.66/–3.92	J71	0.942	14.16	63.80	8.52	[61]
CC10	1.38	–5.72/–4.07	PM6	0.771	22.70	67.30	11.78	[62]

Continued

A-NF-SMA	E_g^{opt} (eV)	HOMO/LUMO (eV)	Donor	V_{oc} (V)	J_{sc} (mA/cm^2)	FF (%)	PCE_{max} (%)	Ref.
N65-IC	1.48	−5.52/−3.89	PBDB-T PBDB-T-2F	0.870 0.870	18.94 15.07	55.00 51.00	9.03 6.67	[63]
N65-2FIC	1.40	−5.60/−4.03	PBDB-T PBDB-T-2F	0.720 0.820	19.11 21.49	62.00 58.00	8.51 10.19	[63]
ITOTC	1.61	−5.66/−3.87	PBDB-T	0.940	15.10	58.82	8.35	[64]
ITUTC	1.60	−5.66/−3.85	PBDB-T	0.940	14.54	56.37	7.68	[64]
ITUIC	1.64	−5.65/−3.83	PBDB-T	0.970	13.64	48.58	6.45	[64]
IOTC	1.69	−5.70/−4.01	PBDB-T	0.950	15.04	55.52	7.94	[66]
IETC	1.72	−5.72/−4.00	PBDB-T	0.960	14.53	53.21	7.40	[66]
IOPC	1.76	−5.71/−3.95	PBDB-T	1.010	10.69	44.90	4.86	[66]
IEPC	1.76	−5.72/−3.96	PBDB-T	1.000	11.55	45.54	5.26	[66]
TIDT-BT-R2	1.68	−5.25/−3.65	PTB7-Th	1.040	13.10	63.90	8.70	[68]
TIDT-BT-R6	1.70	−5.28/−3.67	PTB7-Th	1.030	10.30	52.30	5.60	[68]
PhITBD	– 1.64	−5.74/−3.69 −5.69/−3.99	PTB7-Th PBDB-T	0.757 0.890	14.07 4.560	62.00 44.00	6.57 1.79	[69] [96]
ITBR	1.71	−5.55/−3.71	PTB7-Th	1.020	14.46	51.02	7.49	[29]
ITBRC	1.63	−5.60/−3.82	PTB7-Th	0.790	13.34	59.49	6.27	[29]
ITBC	1.59	−5.64/−3.94	PTB7-Th	0.910	9.21	51.04	4.26	[29]
ITDI	1.36	−5.75/−4.26	PBDB-T	0.940	14.23	60.34	8.00	[72]
CDTDI	1.53	−5.89/−4.18	PBDB-T	0.860	8.16	38.25	2.75	[72]
ITIC-2Cl-β	–	−5.30/−3.71	PBDB-T-2F	0.940	18.47	64.63	11.21	[76]
α-ITIC-2Cl	–	−5.29/−3.77	PBDB-T-2F	0.880	18.91	73.50	12.23	[76]
ITIC-2F	1.56	−5.76/−4.07	PBDB-TF	0.920	17.30	65.70	10.38	[77]
ITIC-3F	1.54	−5.73/−4.12	PBDB-TF	0.890	19.40	66.50	11.44	[77]
a-IT-2OM	1.63	−5.61/−3.92	PBDB-T	0.930	18.11	71.52	12.07	[78]
a-IT-2F	1.56	−5.67/−4.07	PBDB-T	0.780	19.06	68.84	10.28	[78]
IT-3F	–	–	PBDB-TF	0.910	20.33	75.70	13.83	[79]
IDTT-2F-Th	1.55	−5.78/−4.09	PBT1-C-2Cl	0.912	17.82	73.90	12.01	[80]
ITIC-2Cl–Th	–	−5.31/−3.70	PM6	0.860	18.58	72.09	11.45	[81]
ITIC-Cl-γ-Th	–	−5.30/−3.66	PM6	0.910	18.30	73.15	12.25	[81]
ITIC-Cl-δ-Th	–	−5.31/−3.74	PM6	0.890	17.27	72.56	11.13	[81]
ZITI-3F	1.50	−5.64/−3.76	J71	0.900	20.67	71.53	13.15	[82]
IDTBF	1.58	−5.64/−3.80	PM6	0.940	16.98	65.14	10.43	[83]
A1	1.55	−5.15/−3.73	J71	0.970	5.71	29.57	1.63	[84]
A2	1.61	−5.37/−3.67	J71	0.980	11.63	39.63	4.52	[84]
IDT-OB	1.66	−5.77/−3.87	PBDB-T	0.880	16.18	71.10	10.12	[85]
IDTT-OB	1.59	−5.59/−3.88	PBDB-T	0.910	16.19	75.10	11.19	[86]
p-IO1	1.34	−5.46/−4.13	PTB7	0.780	22.30	62.00	10.80	[87]
o-IO1	1.28	−5.44/−4.15	PTB7	0.740	26.30	67.00	13.10	[87]
TOBDT	–	–	PM6	0.890	18.70	68.00	11.30	[88]
MeITBD	1.69	−5.74/−3.95	PBDB-T	0.890	11.10	58.00	5.75	[96]

thermal annealing, reached a PCE of 14.67%.

4.2. A-NF-SMAs with asymmetric terminal groups

Different terminal groups are applied to the A–D–A–D–A structure molecules, and Liu *et al.* developed three kinds of A-NF-SMAS by replacing the fluorine atoms on the terminal groups of Y6 with chlorine atoms (Fig. 11), namely SY1 (two F atoms and one Cl atom), SY2 (two F atoms and two Cl atoms) and SY3 (three Cl atoms). Meanwhile, Y6 with four fluorine atoms substituted terminal groups and Y6-4Cl with four chlorine atoms substituted terminal groups were synthesized as control molecules[90]. Among all acceptors, SY1 has the lowest LUMO energy level and the weakest crystallinity. The results showed that PSCs based on PM6:SY1 blended film yield the champion's PCE was 16.83%, with *V*oc of 0.871 V, J_{sc} of 25.41 mA/cm^2, and FF of 76.0%. Simultaneously, the PCE of devices based on PM6:Y6, PM6:SY2, PM6:SY3, and PM6:Y6-4Cl was 16.19%, 16.01%, 16.23%, and 16.06%, respectively. PM6:SY1-based devices have the best PCEs due to the lowest LUMO energy level of SY1. Besides, more balanced charge transfer, higher charge dissociation and charge collection efficiency, and better morphological characteristics of PM6:SY1-based devices also play an essential role in determining the highest device performance. This contribution indicates that the systematic structure of A-NF-SMAs with different terminal groups can further improve PSCs' PCE.

Luo *et al.* developed a new asymmetric small molecule with one terminal group of BTP-4F and one terminal group of BTP-2ThCl, namely BTP-2F-ThCl (Fig. 11)[91]. In terms of optics, electrochemistry, and crystallinity, BTP-2F-ThCl has similar properties to BTP-4F. BTP-2F-ThCl fine-tunes the acceptor energy level by forming asymmetric terminal groups, so BTP-2F-ThCl achieves a minimal HOMO energy offset and sufficient charge separation. Devices based on BTP-2F-ThCl obtained the best performance of devices based on these three molecules (PCE is 17.06%, *V*oc is 0.869 V, J_{sc} is 25.38 mA/cm^2,

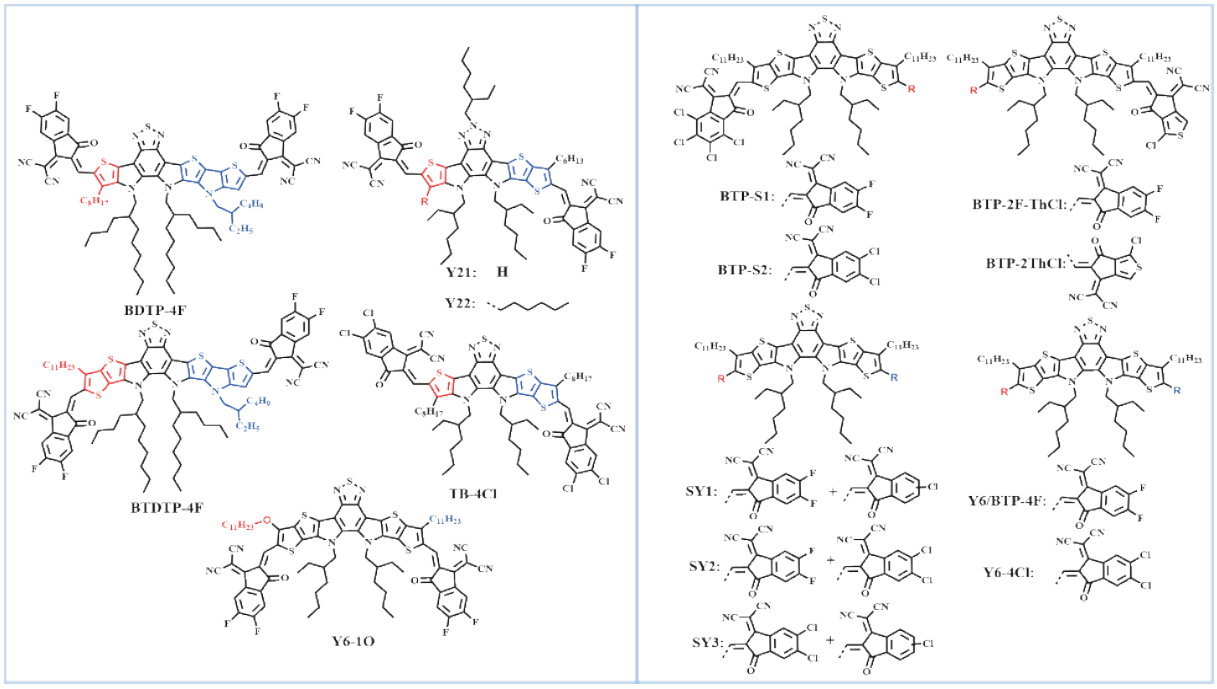

Fig. 11. Chemical structures of asymmetric non-fullerene acceptors based on A1–D–A2–D–A1 structure and the molecules that are associated with them.

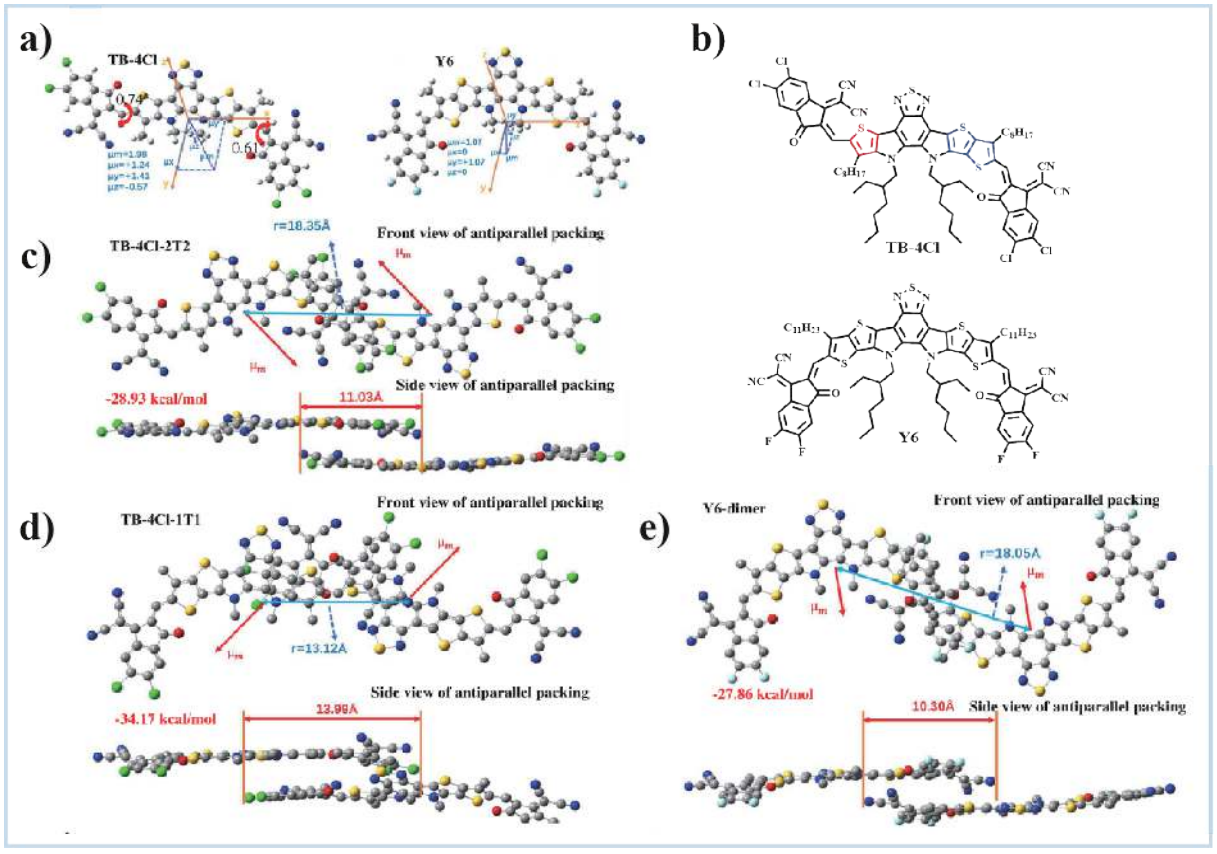

Fig. 12. (a) Molecular conformation of TB-4Cl and Y6. (b) Chemical structures of TB-4Cl and Y6. Models of (c) TB-4Cl-2T2, (d) TB-4Cl-1T1, and (e) Y6-dimer in front view and side view. Reproduced with the permission of Ref. [92].

and FF is 77.4%), which is attributed to the fact that the $V_{oc} \times J_{sc}$ value (22.06) of devices based on BTP-2F-ThCl is greater than that of devices based on BTP-4F (21.18) and BTP-2ThCl (20.76). In the meantime, the PCE_{max} values of BTP-4F-based devices and BTP-2ThCl-based devices are 16.37% and 14.49%, respectively. Li *et al.* introduced halogenated indandione (A1), 3-dicyanomethylene-1-indanone (A2) as two different terminal groups and central core of Y6 to design BTP-S1 and BTP-S2 (Fig. 11)[32]. When the polymer donor PM6 was respectively blended with BTP-S1 and BTP-S2, the blended

Table 2. Device parameters for A–D–A–D–A Typed NF-SMA PSCs.

A-NF-SMA	E_g^{opt} (eV)	HOMO/LUMO (eV)	Donor	V_{oc} (V)	J_{sc} (mA/cm^2)	FF (%)	PCE_{max} (%)	Ref.
BTP-S1	–	–	PM6	0.934	22.39	72.69	15.21	[32]
BTP-S2	–	–	PM6	0.945	24.07	72.02	16.37	[32]
Y6-1O	1.43	–5.71/–3.84	PM6	0.890	23.20	78.30	16.10	[36]
BDTP-4F	1.36	–5.61/–3.90	PM6	0.895	22.54	75.50	15.24	[59]
BTDTP-4F	1.30	–5.56/–3.93	PM6	0.866	21.25	71.30	13.12	[59]
SY1	–	–5.68/–3.95	PM6	0.871	25.41	76.00	16.83	[90]
SY2	–	–5.67/–3.99	PM6	0.852	25.29	74.30	16.01	[90]
SY3	–	–5.69/–3.98	PM6	0.858	25.54	74.10	16.23	[90]
BTP-2F-ThCl	1.34	–5.70/–3.99	PM6	0.869	25.38	77.40	17.06	[91]
TB-4Cl	–	–5.70/–4.10	PM6 PM7	0.848 0.862	22.16 21.67	75.20 71.78	14.67 13.67	[92]
Y21	1.35	–5.65/–3.90	PM6	0.830	24.90	74.40	15.40	[93]
Y22	1.38	–5.69/–3.94	PM6	0.853	24.37	74.12	15.40	[94]

films showed excellent photovoltaic performance. Energy loss analysis shows that device corresponding to the asymmetric molecule BTP-S2 with six chlorine atoms at the end has better electroluminescence quantum efficiency (2.3×10^{-2} %) than the device corresponding to the symmetric molecule Y6 (4.4×10^{-3} %), which results in BTP-S2-based device with low non-radiation loss of 0.22 eV. Besides, asymmetric BTP-S1 and BTP-S2 with multiple halogen atoms at the end can lead to more efficient charge separation. The optimized devices for PM6:Y6:BTP-S2, PM6:BTP-S2 and PM6:Y6 blends yield comparable PCEs of 17.43%, 16.37% and 15.79%, this result proves that the ternary hybrid strategy can improve the performance of PSCs more than the binary hybrid strategy. Ultimately, the PCE of PSCs based on PM6:BTP-S2 was 16.37%, which was higher than that of PSCs based on PM6:Y6 (15.79%), which showed the effectiveness of the asymmetric design.

4.3. A-NF-SMAs with asymmetric side chains

The branched alkyl chain has a significant influence on the solubility of the molecule and morphology of the mixed film, which will make the final device have different properties. Chen *et al.* applied asymmetric alkyl and alkoxy substitution strategies to the most advanced y-series non-fullerene acceptors and obtained a type of A-NF-SMA named Y6-1O (Fig. 11)[36]. If an alkoxy chain symmetrically modifies Y6, the resulting molecule will show low solubility and excessive aggregation due to its conformational locking effect. Y6-1O chooses asymmetric alkyl and alkoxy substituents, which can balance the harmful effects of the alkoxy chain while maintaining the beneficial electronic effects of the alkoxy group. It can achieve quite a good solubility (20 mg/mL) and morphology. Y6-1O can maintain the positive effect of *V*oc improvement and obtain quite a good solubility, which helps Y6-1O-based devices to obtain high V_{oc} (0.89 V), J_{sc} (23.2 mA/cm^2) and FF (78.3%). Therefore, the best PCE of PM6:Y6-1O-based devices is as high as 16.1%. Further addition of $PC_{71}BM$ to the binary blend will result in a higher PCE of the device (17.6%).

The study of A–D–A–D–A typed asymmetric non-fullerene small molecules thoroughly explored the critical role of molecular conformation regulation on morphology and device efficiency, which has important guiding significance for the molecular design of NF-SMAs.

Table 2 shows the performance parameters of A–D–A–D–A typed A-NF-PSCs.

5. Conclusion and future outlook

For A–D–A typed asymmetric non-fullerene small molecules:

a) In the asymmetry of the core, molecules with DTP units show great potential. The device fabricated based on A-NF-SMA TPIC-4Cl with DTP unit obtained a PCEmax of 15.31%, which is the highest PCE_{max} in the A–D–A-type A-NF-PSCs so far. b) The "one-pot synthesis of mixed materials" strategy provides new ideas for molecular design, which can significantly reduce the device complexity of the traditional ternary strategy. ZITI-m is a mixture of A-NF-SMA ZITI-3F and S-NF-SMA ZITI-4F synthesized by the "one-pot Knoevenagel reaction". Compared with ZITI-3F and ZITI-4F, the PSC of the hybrid materials ZITI-m and J71 shows a very high PCE_{max} (13.65%). c) Side-chain asymmetric molecules are expected to further improve device performance, and research in this area should receive more attention. So far, reports on side-chain asymmetry only include 6 molecules IDT-OB, IDTT-OB, P-IO1, O-IO1, TOBDT and Y6-1O. Relative to core asymmetry and terminal group asymmetry, the number of studies related to these molecules is very small. However, the PCE_{max} values of these molecular-related devices are 10.12%, 11.19%, 10.80%, 13.10%, and 11.30%, which are all greater than 10%, showing great potential in the field of PSCs.

For A–D–A–D–A typed asymmetric non-fullerene small molecules:

a) Substituting thiophene for the benzene ring at the fluorinated IC terminal to form a new terminal T-IC, and using both the fluorinated IC terminal and the T-IC terminal group in the asymmetric A unit in A-NF-SMA has broad application prospects. The BTP-2F-ThCl synthesized by this move and the PSC fabricated after blending with the donor PM6 have reached the best PCE_{max} (17.06%) of the recent binary device. b) Fabrication of ternary PSCs also is a promising strategy further to improve the photovoltaic performance of binary PSCs. This article refers to the PCE_{max} of PSCs of the ternary blend (PM6:Y6:BTP-S2) was 17.43%, which improved the binary device's performance of PSCs based on PM6:BTP-S2 and PM6:Y6 (PCE_{max} = 16.37%, 15.79%).

In short, the asymmetric design of the molecule has the following advantages:

1) It helps increase the dipole moment and dielectric constant of the molecule and reduces the binding energy of excitons, which is very beneficial for exciton dissociation and

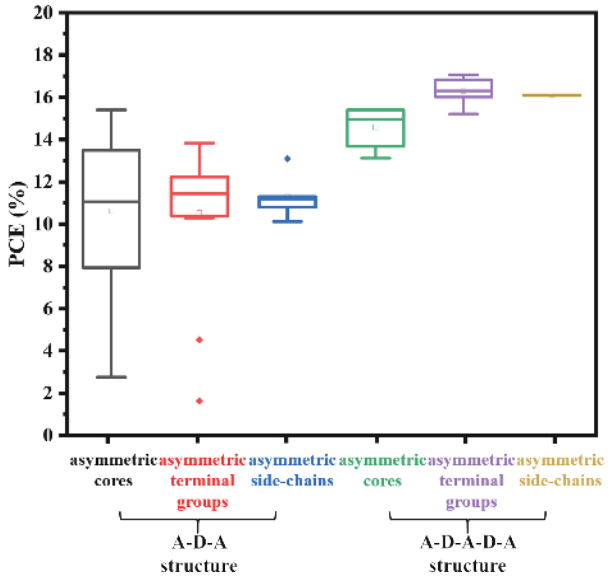

Fig. 13. The box chart of PCE distribution for A-NF-SMAs based on different structures.

charge transport. 2) The asymmetric structure design will also fine-tune the molecular energy level to adjust the V_{oc} further. The influence on the absorption range and absorption intensity will cause the J_{sc} to change. The $V_{oc} \times J_{sc}$ value can be further optimized through the asymmetric molecular design, resulting in higher device performance. 3) The effect on molecular aggregation and molecular stacking can directly change the microscopic morphology, phase separation size, and the active layer's crystallinity.

However, the synthesis of A-NF-SMAs is more complicated and costly, which is a big problem that scientists will face in the future. The box chart of PCE distribution for A-NF-SMAs is shown in Fig. 13, which records the latest developments in A-NF-SMAs based on different structures. The structural modularity of small molecules facilitates molecular tailoring and property regulation. This advantage can enable the continuous development of A-NF-SMAs in interface engineering, shape control and device structure optimization research, which will further promote the development of PSCs.

Acknowledgments

The authors acknowledge financial support from the National Key R&D Program of "Strategic Advanced Electronic Materials" (No.2016YFB0401100), the National Natural Science Foundation of China (Grant No.61574077), Major Program of Natural Science Foundation of the Higher Education Institutions of Jiangsu Province, China (No.19KJA460005) and Natural Science Foundation of Jiangsu Province (BK20170961).

References

[1] Winzenberg K N, Kemppinen P, Scholes F H, et al. Indan-1, 3-dione electron-acceptor small molecules for solution-processable solar cells: A structure-property correlation. Chem Commun, 2013, 49, 6307

[2] Zhou T L, Jia T, Kang B N, et al. Nitrile-substituted QA derivatives: New acceptor materials for solution-processable organic bulk heterojunction solar cells. Adv Energy Mater, 2011, 1, 431

[3] Fang Y, Pandey A K, Nardes A M, et al. A narrow optical gap small molecule acceptor for organic solar cells. Adv Energy Mater, 2013, 3, 54

[4] Nielsen C B, Voroshazi E, Holliday S, et al. Efficient truxenone-based acceptors for organic photovoltaics. J Mater Chem A, 2013, 1, 73

[5] Bloking J T, Han X, Higgs A T, et al. Solution-processed organic solar cells with power conversion efficiencies of 2.5% using benzothiadiazole/imide-based acceptors. Chem Mater, 2011, 23, 5484

[6] Lin Y Z, Wang H F, Li Y F, et al. A star-shaped electron acceptor based on 5, 5'-bibenzothiadiazole for solution processed solar cells. J Mater Chem A, 2013, 1, 14627

[7] Lin Y Z, Cheng P, Li Y F, et al. A 3D star-shaped non-fullerene acceptor for solution-processed organic solar cells with a high open-circuit voltage of 1.18 V. Chem Commun, 2012, 48, 4773

[8] Li J F, Sun C K, Tang A L, et al. Utilizing an electron-deficient thieno[3, 4-c]pyrrole-4, 6-dione (TPD) unit as a π-bridge to improve the photovoltaic performance of A–π–D–π–A type acceptors. J Mater Chem C, 2020, 8, 15981

[9] Wang J Y, Zhan X W. Fused-ring electron acceptors for photovoltaics and beyond. Acc Chem Res, 2021, 54, 132

[10] Chen W Q, Zhang Q C. Recent progress in non-fullerene small molecule acceptors in organic solar cells (OSCs). J Mater Chem C, 2017, 5, 1275

[11] Sun H, Song X, Xie J, et al. PDI derivative through fine-tuning the molecular structure for fullerene-free organic solar cells. ACS Appl Mater Interfaces, 2017, 9, 29924

[12] Fan X B, Gao J H, Wang W, et al. Ladder-type nonacyclic arene bis(thieno[3, 2-b]thieno)cyclopentafluorene as a promising building block for non-fullerene acceptors. Chem Asian J, 2019, 14, 1814

[13] Liu Q S, Jiang Y F, Jin K, et al. 18% efficiency organic solar cells. Sci Bull, 2020, 65, 272

[14] Lin Y Z, Wang J Y, Zhang Z G, et al. An electron acceptor challenging fullerenes for efficient polymer solar cells. Adv Mater, 2015, 27, 1170

[15] Lin Y Z, Li Y F, Zhan X W. A solution-processable electron acceptor based on dibenzosilole and diketopyrrolopyrrole for organic solar cells. Adv Energy Mater, 2013, 3, 724

[16] Li H Y, Earmme T, Ren G Q, et al. Beyond fullerenes: Design of nonfullerene acceptors for efficient organic photovoltaics. J Am Chem Soc, 2014, 136, 14589

[17] Sharenko A, Proctor C M, van der Poll T S, et al. A high-performing solution-processed small molecule: Perylene diimide bulk heterojunction solar cell. Adv Mater, 2013, 25, 4403

[18] Lin Y Z, Zhao F W, Wu Y, et al. Mapping polymer donors toward high-efficiency fullerene free organic solar cells. Adv Mater, 2017, 29, 1604155

[19] Chen X, Zheng S H. On the study of influence of molecular arrangements and dipole moment on exciton binding energy in solid state. Int J Quantum Chem, 2021, 121, e26511

[20] Benatto L, de Almeida Sousa K R, Koehler M. Driving force for exciton dissociation in organic solar cells: The influence of donor and acceptor relative orientation. J Phys Chem C, 2020, 124, 13580

[21] Cao J R, Qu S Y, Yang L Q, et al. An asymmetric acceptor enabling 77.51% fill factor in organic solar cells. Sci Bull, 2020, 65, 1876

[22] Ma R J, Liu T, Luo Z H, et al. Adding a third component with reduced miscibility and higher LUMO level enables efficient ternary organic solar cells. ACS Energy Lett, 2020, 5, 2711

[23] Yin L X, Yuan Q Q, Li Y Q. D–A–A'-type asymmetric small molecules based on triphenylamine-diketopyrrolopyrrole/5, 6-difluoro-2, 1, 3-benzothiadiazole backbone for organic photovoltaic materials. New J Chem, 2020, 44, 13319

[24] Congreve D N, Lee J, Thompson N J, et al. External quantum efficiency above 100% in a singlet-exciton-fission-based organic photovoltaic cell. Science, 2013, 340, 334

[25] Schwenn P E, Gui K, Nardes A M, et al. A small molecule non-fullerene electron acceptor for organic solar cells. Adv Energy Mater, 2011, 1, 73
[26] Shu Y, Lim Y F, Li Z, et al. A survey of electron-deficient pentacenes as acceptors in polymer bulk heterojunction solar cells. Chem Sci, 2011, 2, 363
[27] Zhou Y, Ding L, Shi K, et al. A non-fullerene small molecule as efficient electron acceptor in organic bulk heterojunction solar cells. Adv Mater, 2012, 24, 957
[28] Li C, Fu H T, Xia T, et al. Asymmetric nonfullerene small molecule acceptors for organic solar cells. Adv Energy Mater, 2019, 9, 1900999
[29] Tang C Q, Chen S C, Shang Q, et al. Asymmetric indenothiophene-based non-fullerene acceptors for efficient polymer solar cells. Sci China Mater, 2017, 60, 707
[30] Yuan J, Zhang Y Q, Zhou L Y, et al. Single-junction organic solar cell with over 15% efficiency using fused-ring acceptor with electron-deficient core. Joule, 2019, 3, 1140
[31] Guo X, Fan Q P, Wu J N, et al. Optimized active layer morphologies via ternary copolymerization of polymer donors for 17.6 % efficiency organic solar cells with enhanced fill factor. Angew Chem Int Ed, 2021, 60, 2322
[32] Li S X, Zhan L L, Jin Y Z, et al. Asymmetric electron acceptors for high-efficiency and low-energy-loss organic photovoltaics. Adv Mater, 2020, 32, 2001160
[33] Zhang C X, Liu R G, Mak C H, et al. Photophysics of organic photovoltaic devices: A review. J Photonics Energy, 2018, 8, 021001
[34] Ilmi R, Haque A, Khan M S. High efficiency small molecule-based donor materials for organic solar cells. Org Electron, 2018, 58, 53
[35] Qi B, Wang J. Fill factor in organic solar cells. Phys Chem Chem Phys, 2013, 15, 8972
[36] Chen Y Z, Bai F J, Peng Z X, et al. Asymmetric alkoxy and alkyl substitution on nonfullerene acceptors enabling high-performance organic solar cells. Adv Energy Mater, 2021, 11, 2003141
[37] Li C, Xie Y P, Fan B B, et al. A nonfullerene acceptor utilizing a novel asymmetric multifused-ring core unit for highly efficient organic solar cells. J Mater Chem C, 2018, 6, 4873
[38] Song J L, Li C, Ye L L, et al. Extension of indacenodithiophene backbone conjugation enables efficient asymmetric A–D–A type nonfullerene acceptors. J Mater Chem A, 2018, 6, 18847
[39] Liu S N, Zhao B F, Cong Z Y, et al. Influences of the terminal groups on the performances of asymmetric small molecule acceptors-based polymer solar cells. Dyes Pigments, 2020, 178, 108388
[40] Gao W, Liu T, Zhong C, et al. Asymmetrical small molecule acceptor enabling nonfullerene polymer solar cell with fill factor approaching 79%. ACS Energy Lett, 2018, 3, 1760
[41] Li X S, Li C, Ye L L, et al. Asymmetric A–D–π–A-type nonfullerene small molecule acceptors for efficient organic solar cells. J Mater Chem A, 2019, 7, 19348
[42] Gao W, Zhang M, Liu T, et al. Asymmetrical ladder-type donor-induced polar small molecule acceptor to promote fill factors approaching 77% for high-performance nonfullerene polymer solar cells. Adv Mater, 2018, 30, 1800052
[43] Gao W, Wu F, Liu T, et al. Multifunctional asymmetrical molecules for high-performance perovskite and organic solar cells. J Mater Chem A, 2019, 7, 2412
[44] Gao W, Liu T, Sun R, et al. Dithieno[3, 2-b: 2′, 3′-d]pyrrol-fused asymmetrical electron acceptors: A study into the effects of nitrogen-functionalization on reducing nonradiative recombination loss and dipole moment on morphology. Adv Sci, 2020, 7, 1902657
[45] Gao W, An Q S, Zhong C, et al. Designing an asymmetrical isomer to promote the LUMO energy level and molecular packing of a non-fullerene acceptor for polymer solar cells with 12.6% efficiency. Chem Sci, 2018, 9, 8142
[46] Li C, Song J L, Ye L L, et al. High-performance eight-membered indacenodithiophene-based asymmetric A-D-A type non-fullerene acceptors. Sol RRL, 2019, 3, 1800246
[47] Li C, Song J L, Cai Y H, et al. Heteroatom substitution-induced asymmetric A-D-A type non-fullerene acceptor for efficient organic solar cells. J Energy Chem, 2020, 40, 144
[48] Li C, Xia T, Song J L, et al. Asymmetric selenophene-based nonfullerene acceptors for high-performance organic solar cells. J Mater Chem A, 2019, 7, 1435
[49] Wang X C, Han J H, Jiang H X, et al. Regulation of molecular packing and blend morphology by finely tuning molecular conformation for high-performance nonfullerene polymer solar cells. ACS Appl Mater Interfaces, 2019, 11, 44501
[50] Gao W, Liu T, Li J W, et al. Simultaneously increasing open-circuit voltage and short-circuit current to minimize the energy loss in organic solar cells via designing asymmetrical non-fullerene acceptor. J Mater Chem A, 2019, 7, 11053
[51] Zhang X M, Li M M, Wang Q, et al. Near-infrared absorbing nonfullerene acceptors with dithienopyrrole as π spacer for organic solar cells. Chin J Appl Chem, 2019, 36, 1023
[52] Geng Y F, Tang A L, Tajima K, et al. Conjugated materials containing dithieno[3, 2-b: 2', 3'-d]pyrrole and its derivatives for organic and hybrid solar cell applications. J Mater Chem A, 2019, 7, 64
[53] Yang L Q, Song X, Yu J S, et al. Tuning of the conformation of asymmetric nonfullerene acceptors for efficient organic solar cells. J Mater Chem A, 2019, 7, 22279
[54] Yang L Q, Hu Z H, Zhang Z H, et al. Molecular engineering of acceptors to control aggregation for optimized nonfullerene solar cells. J Mater Chem A, 2020, 8, 5458
[55] Ma R J, Li G, Li D D, et al. Understanding the effect of end group halogenation in tuning miscibility and morphology of high-performance small molecular acceptors. Sol RRL, 2020, 4, 2000250
[56] Li G, Li D D, Ma R J, et al. Efficient modulation of end groups for the asymmetric small molecule acceptors enabling organic solar cells with over 15% efficiency. J Mater Chem A, 2020, 8, 5927
[57] Cao J R, Qu S Y, Yu J S, et al. 13.76% efficiency nonfullerene solar cells enabled by selenophene integrated dithieno[3, 2-b:2', 3'-d]pyrrole asymmetric acceptors. Mater Chem Front, 2020, 4, 924
[58] Guo Q, Ma R J, Hu J, et al. Over 15% efficiency polymer solar cells enabled by conformation tuning of newly designed asymmetric small-molecule acceptors. Adv Funct Mater, 2020, 30, 2000383
[59] Luo Z H, Ma R J, Xiao Y Q, et al. Conformation-tuning effect of asymmetric small molecule acceptors on molecular packing, interaction, and photovoltaic performance. Small, 2020, 16, 2001942
[60] Zhang Z H, Yang L Q, Hu Z H, et al. Charge density modulation on asymmetric fused-ring acceptors for high-efficiency photovoltaic solar cells. Mater Chem Front, 2020, 4, 1747
[61] Luo Z H, Li G H, Wu K L, et al. Asymmetric thieno[2, 3-b]thiophene-based electron acceptor featuring a seven fused-ring electron donor unit as core for nonfullerene organic photovoltaics. Org Electron, 2018, 62, 82
[62] Jiao C C, Guo Z Q, Sun B Q, et al. An acceptor–donor–acceptor type non-fullerene acceptor with an asymmetric backbone for high performance organic solar cells. J Mater Chem C, 2020, 8, 6293
[63] Hu W, Du X Y, Zhuang W L, et al. Axisymmetric and asymmetric naphthalene-bisthienothiophene based nonfullerene acceptors: On constitutional isomerization and photovoltaic performance. ACS Appl Energy Mater, 2020, 3, 5734
[64] Zhang M Q, Ma Y L, Zheng Q D. Asymmetric indenothienothiophene-based unfused core for A-D-A type nonfullerene acceptors. Dyes Pigments, 2020, 180, 108495
[65] Huang B, Chen L, Jin X F, et al. Alkylsilyl functionalized copolymer donor for annealing-free high performance solar cells with over 11% efficiency: Crystallinity induced small driving force. Adv Funct Mater, 2018, 28, 1800606
[66] Kang Z J, Ma Y L, Zheng Q D. Asymmetric indenothiophene-

based nonfullerene acceptors for binary- and ternary-blend polymer solar cells. Dyes Pigments, 2019, 170, 107555
[67] Hong L, Yao H F, Yu R N, et al. Investigating the trade-off between device performance and energy loss in nonfullerene organic solar cells. ACS Appl Mater Interfaces, 2019, 11, 29124
[68] Bai W Y, Xu X P, Li Q Y, et al. Efficient nonfullerene polymer solar cells enabled by small-molecular acceptors with a decreased fused-ring core. Small Methods, 2018, 2, 1700373
[69] Un Kim Y, Eun Park G, Choi S, et al. A new n-type semiconducting molecule with an asymmetric indenothiophene core for a high-performing non-fullerene type organic solar cell. J Mater Chem C, 2017, 5, 7182
[70] Li Q Y, Xiao J Y, Tang L M, et al. Thermally stable high performance non-fullerene polymer solar cells with low energy loss by using ladder-type small molecule acceptors. Org Electron, 2017, 44, 217
[71] Xiao J Y, Chen Z M, Zhang G C, et al. Efficient device engineering for inverted non-fullerene organic solar cells with low energy loss. J Mater Chem C, 2018, 6, 4457
[72] Kang Z J, Chen S C, Ma Y L, et al. Push-pull type non-fullerene acceptors for polymer solar cells: Effect of the donor core. ACS Appl Mater Interfaces, 2017, 9, 24771
[73] Zhang Y, Wang Y, Xie Z Y, et al. Preparation of non-fullerene acceptors with a multi-asymmetric configuration in a one-pot reaction for organic solar cells. J Mater Chem C, 2020, 8, 17229
[74] Hu D Q, Yang Q G, Zheng Y J, et al. 15.3% efficiency all-small-molecule organic solar cells achieved by a locally asymmetric F, Cl disubstitution strategy. Adv Sci, 2021, 8, 2004262
[75] Pan F, Li X J, Bai S, et al. High electron mobility fluorinated indacenodithiophene small molecule acceptors for organic solar cells. Chin Chem Lett, 2021, 32, 1257
[76] Lai H J, Chen H, Zhou J D, et al. 3D interpenetrating network for high-performance nonfullerene acceptors via asymmetric chlorine substitution. J Phys Chem Lett, 2019, 10, 4737
[77] Aldrich T J, Matta M, Zhu W, et al. Fluorination effects on indacenodithienothiophene acceptor packing and electronic structure, end-group redistribution, and solar cell photovoltaic response. J Am Chem Soc, 2019, 141, 3274
[78] Li M, Zhou Y Y, Zhang J Q, et al. Tuning the dipole moments of nonfullerene acceptors with an asymmetric terminal strategy for highly efficient organic solar cells. J Mater Chem A, 2019, 7, 8889
[79] Gao B W, Yao H F, Hou J X, et al. Multi-component non-fullerene acceptors with tunable bandgap structures for efficient organic solar cells. J Mater Chem A, 2018, 6, 23644
[80] Ye L L, Xie Y P, Xiao Y Q, et al. Asymmetric fused-ring electron acceptor with two distinct terminal groups for efficient organic solar cells. J Mater Chem A, 2019, 7, 8055
[81] Lai H J, Chen H, Shen Y, et al. Using chlorine atoms to fine-tune the intermolecular packing and energy levels of efficient nonfullerene acceptors. ACS Appl Energy Mater, 2019, 2, 7663
[82] Zhang J Y, Liu W R, Chen S S, et al. One-pot synthesis of electron-acceptor composite enables efficient fullerene-free ternary organic solar cells. J Mater Chem A, 2018, 6, 22519
[83] Duan T N, Hou L C, Fu J H, et al. An asymmetric end-capping strategy enables a new non-fullerene acceptor for organic solar cells with efficiency over 10%. Chem Commun, 2020, 56, 6531
[84] Zhao Y, Luo Z H, Li G H, et al. De novo design of small molecule acceptors via fullerene/non-fullerene hybrids for polymer solar cells. Chem Commun, 2018, 54, 9801
[85] Feng S Y, Zhang C E, Liu Y H, et al. Fused-ring acceptors with asymmetric side chains for high-performance thick-film organic solar cells. Adv Mater, 2017, 29, 1703527
[86] Feng S Y, Zhang C, Bi Z Z, et al. Controlling molecular packing and orientation via constructing a ladder-type electron acceptor with asymmetric substituents for thick-film nonfullerene solar cells. ACS Appl Mater Interfaces, 2019, 11, 3098
[87] Lee J, Song S, Huang J F, et al. Bandgap tailored nonfullerene acceptors for low-energy-loss near-infrared organic photovoltaics. ACS Mater Lett, 2020, 2, 395
[88] Chen X B, Kan B, Kan Y Y, et al. As-cast ternary organic solar cells based on an asymmetric side-chains featured acceptor with reduced voltage loss and 14.0% efficiency. Adv Funct Mater, 2020, 30, 1909535
[89] Liu X Z, Wei Y N, Zhang X, et al. An A-D-A'-D-A type unfused nonfullerene acceptor for organic solar cells with approaching 14% efficiency. Sci China Chem, 2021, 64, 228
[90] Liu T, Zhang Y D, Shao Y M, et al. Asymmetric acceptors with fluorine and chlorine substitution for organic solar cells toward 16.83% efficiency. Adv Funct Mater, 2020, 30, 2000456
[91] Luo Z H, Ma R J, Liu T, et al. Fine-tuning energy levels via asymmetric end groups enables polymer solar cells with efficiencies over 17%. Joule, 2020, 4, 1236
[92] Zhang J S, Han Y F, Zhang W X, et al. High-efficiency thermal-annealing-free organic solar cells based on an asymmetric acceptor with improved thermal and air stability. ACS Appl Mater Interfaces, 2020, 12, 57271
[93] Cai F F, Zhu C, Yuan J, et al. Efficient organic solar cells based on a new "Y-series" non-fullerene acceptor with an asymmetric electron-deficient-core. Chem Commun, 2020, 56, 4340
[94] Cai F F, Peng H J, Chen H G, et al. An asymmetric small molecule acceptor for organic solar cells with a short circuit current density over 24 mA cm^{-2}. J Mater Chem A, 2020, 8, 15984
[95] Zhang M, Gao W, Zhang F J, et al. Efficient ternary non-fullerene polymer solar cells with PCE of 11.92% and FF of 76. 5%. Energy Environ Sci, 2018, 11, 841
[96] Jeong C H, Kim Y U, Park C G, et al. Improved performance of non-fullerene polymer solar cells by simple structural change of asymmetric acceptor based on indenothiophene. Synth Met, 2018, 246, 164

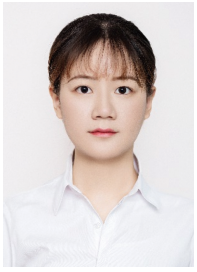

Liu Ye received a B.S. degree in applied chemistry from Xinzhou Teachers University in 2019. Now, she is an M.E. student at the Institute of Advanced Materials (IAM), Nanjing Tech University. Her research interest focuses on asymmetric non-fullerene small molecule acceptors for polymer solar cells.

Shiming Zhang received his PhD in 2009 from the Institute of Chemistry, Chinese Academy of Sciences, and subsequently began two years of postdoctoral research within the Department of Chemistry at Northwestern University under the supervision of Prof. Tobin J. Marks and Antonio Facchetti. He worked at KAUST (Saudi Arabia) as a postdoctoral fellow from 2011 to 2012, after which he moved to Singapore to work in Silecs International as a senior chemist from 2012 to 2014 and WinTech Nano as a quality lead/principal engineer from 2014 to 2015. In 2015 he joined the Institute of Advanced Materials (IAM) and began his professorship at Nanjing Tech University (NanjingTech) as a professor. His research interests include organic/flexible electronics and microelectronics-packaging materials.